

Design, Synthesis, Biological Activity, and ADME Properties of Pyrazolo[3,4-*d*]pyrimidines Active in Hypoxic Human Leukemia Cells: A Lead Optimization Study

Marco Radi,[†] Elena Dreassi,[†] Chiara Brullo,[‡] Emmanuele Crespan,^{||} Cristina Tintori,[†] Vincenzo Bernardo,[†] Massimo Valoti,[#] Claudio Zamperini,[†] Henry Daigl,[†] Francesca Musumeci,[‡] Fabio Carraro,[§] Antonella Naldini,[§] Irene Filippi,[§] Giovanni Maga,^{||} Silvia Schenone,^{*,‡} and Maurizio Botta^{*,†,‡}

[†]Dipartimento Farmaco Chimico Tecnologico, University of Siena, Via Alcide de Gasperi 2, I-53100 Siena, Italy

[#]Sbarro Institute for Cancer Research and Molecular Medicine, Center for Biotechnology, College of Science and Technology, Temple University, BioLife Science Building, Suite 333, 1900 N 12th Street, Philadelphia, Pennsylvania 19122, United States

[§]Dipartimento di Fisiologia, Sezione di Neuroimmunofisiologia, University of Siena, Via Aldo Moro, I-53100 Siena, Italy

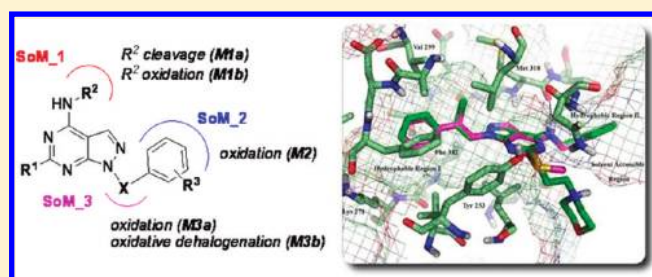
^{||} Istituto di Genetica Molecolare, IGM-CNR, Via Abbiategrosso 207, I-27100 Pavia, Italy

[‡]Dipartimento di Scienze Farmaceutiche, University of Genoa, Viale Benedetto XV 3, I-16132 Genova, Italy

^{*}Dipartimento di Neuroscienze, University of Siena, Via Alcide de Gasperi 2, I-53100 Siena, Italy

S Supporting Information

ABSTRACT: A family of dual Src/Abl inhibitors characterized by a substituted pyrazolo[3,4-*d*]pyrimidine scaffold was previously reported by us and proved to be active against several tumor cell lines. Among these compounds, a promising antileukemia lead (**1**) has been recently identified, but, unfortunately, it suffers from substandard pharmaceutical properties. Accordingly, an approach for the optimization of the lead **1** is described in the present work. A series of more soluble pyrazolo[3,4-*d*]pyrimidine derivatives were rationally designed and proved to maintain the dual Src/Abl activity of the lead. Selected compounds showed an interesting activity profile against three different leukemic cells also in hypoxic conditions, which are usually characterized by imatinib-resistance. Finally, *in vitro* ADME properties (PAMPA permeation, water solubility, microsomal stability) for the most promising inhibitors were also evaluated, thus allowing the identification of a few optimized analogues of lead **1** as promising antileukemia agents.

**INTRODUCTION**

Chronic myeloid leukemia (CML) is a hematopoietic stem cell cancer that arises following a reciprocal genetic translocation between chromosomes 9 and 22.¹ This translocation produces the Philadelphia (Ph) chromosome that encodes for a constitutively activated fusion protein: the oncogenic tyrosine kinase Bcr-Abl.² The understanding of the central role played by Bcr-Abl in the pathogenesis of CML gave birth to the so-called “targeted therapy” that culminated with the FDA-approval of imatinib (IM) (Figure 1), currently used as frontline therapy.³ The initial enthusiasm generated by the high response rate to IM-treatment was, however, dampened by the insurgence of drug resistance, especially in the advanced phases of the disease, which can be caused by both Bcr-Abl-dependent mechanisms (e.g., point mutations in the kinase domain of the enzyme and Bcr-Abl gene amplification) and Bcr-Abl-independent mechanisms (activation of alternative pathways, e.g., Src family kinases).⁴ Despite the fact that the targeted therapy era started as a hunt for selective kinase

inhibitors,⁵ the aim has recently changed to the identification of compounds acting on multiple targets (dirty drugs) in order to overcome the drug resistance often connected to the activation of alternative signaling pathways.⁶ Multitargeted cancer chemotherapy was, in fact, proven to be very effective in treating a number of tumors such as breast, prostate, and esophageal cancer. Examples of multikinase inhibitors currently used in anticancer therapy can be represented by Sunitinib (which targets PDGFRs, VEGFRs, RET, CSF1R, FLT3, and c-Kit), approved for the treatment of renal cell carcinoma and IM-resistant gastrointestinal stromal tumor, and Sorafenib (which targets PDGFRs, VEGFRs, c-Kit, and RAF), approved for the treatment of renal cell carcinoma and hepatocellular carcinoma (Figure 1).⁷ IM itself has been shown to act not only on Bcr-Abl but also on c-Kit and PDGFR kinases.⁸ An alternative approach

Received: October 5, 2010

Published: March 28, 2011

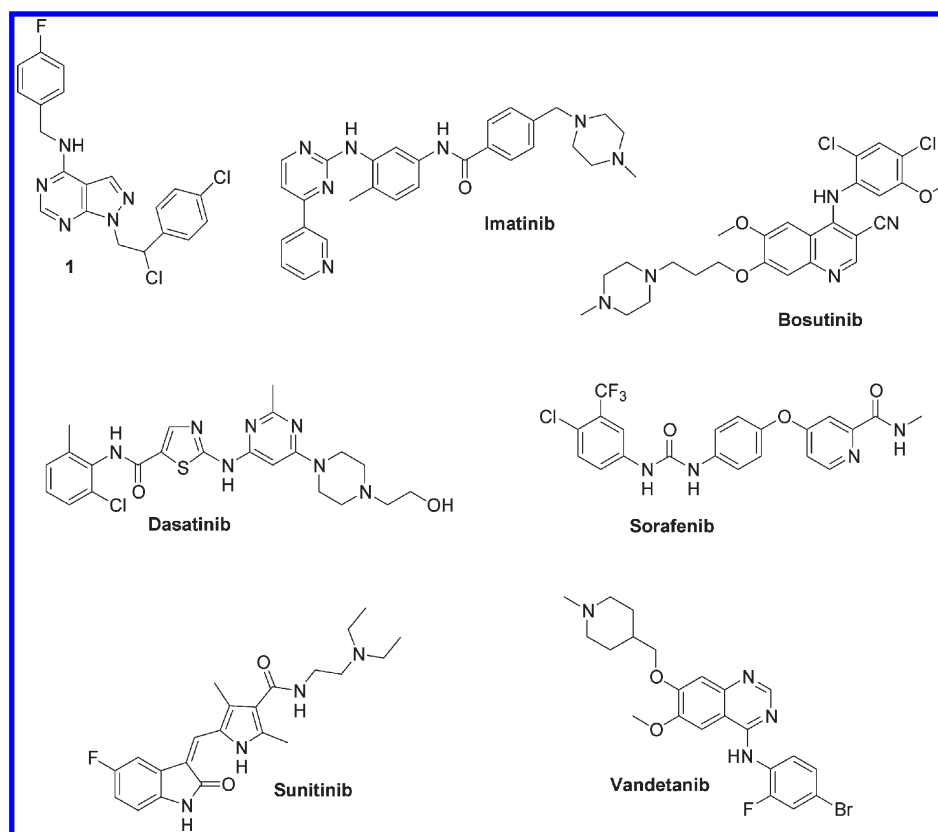


Figure 1. Selected first- and second-generation TKIs.

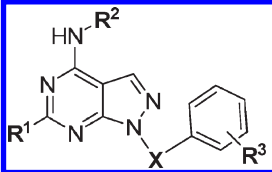
has been recently investigated to overcome the drug resistance to common ATP-competitive inhibitors: compounds targeting sites outside the ATP-binding cleft (allosteric inhibitors) have been identified and proven effective against IM-sensitive and IM-resistant leukemic cells both alone and in combination with common drugs.⁹

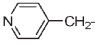
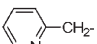
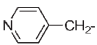
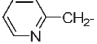
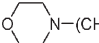
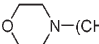
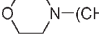
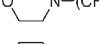
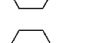

Among the many proteins targeted by the kinase inhibitors, c-Src (hereinafter referred to as Src) proved to play an important accessory role in the field of leukemia: studies with Src dominant-negative mutants in fact provided enough evidence to implicate Src in the proliferation of Bcr-Abl-expressing cells, while its overexpression seems to be implicated in Bcr-Abl-mediated leukaemogenesis and IM-resistance.¹⁰ Moreover, since Src shares significant sequence homology and remarkable structural resemblance with the active form of Abl, several Src inhibitors showed potent Bcr-Abl inhibitory activity and were successfully used as second generation antileukemia drugs. This approach allowed the identification of dual Src/Abl inhibitors such as Dasatinib and Bosutinib, which are effective drugs for the treatment of IM-resistant patients (Figure 1).¹¹ The significance of dual Src/Abl inhibition in overcoming IM-resistance has been recently highlighted by König and colleagues: Dasatinib showed in fact potent Src inhibition in CML progenitors, inhibiting both Bcr-Abl-dependent and -independent Src activity, in contrast to IM that inhibited only Bcr-Abl-dependent Src activity.¹² The importance of Src inhibition in CML treatment has also been confirmed by a recent study on the antiangiogenic compound ZD6474 (Vandetanib) (Figure 1), which has been found responsible for the growth arrest and apoptosis in IM-sensitive and IM-resistant leukemic K-562 cells.¹³ Another important factor responsible for drug resistance is represented by the presence of

specific niches within the bone marrow microenvironment where a subpopulation of leukemic cells can evade chemotherapy and acquire a drug-resistant phenotype.¹⁴ Leukemic cells infiltrating the bone marrow in rats proved to be markedly hypoxic and were able to proliferate in virtue of their adaption capacity to the hypoxic microenvironment.¹⁵ Although hypoxia is known to be associated with both radio- and chemoresistance in solid tumors, its role in leukemia has been poorly investigated, particularly in the context of resistance to targeted therapies. A very interesting study has recently shown that hypoxia-selected CML cells did not express the Bcr-Abl protein, thereby accounting for their complete resistance to IM treatment.¹⁶ It has, therefore, been suggested that a reliable biological evaluation of antileukemic compounds should account for the “*in situ* normoxia” conditions:¹⁷ for the bone marrow compartment, this oxygen concentration has been estimated at from 0% to 4%.¹⁸

In the past few years, our research group has conducted extensive studies on a new family of dual Src/Abl inhibitors endowed with a pyrazolo[3,4-*d*]pyrimidine scaffold. Several members of this family were found to induce apoptosis and reduce cell proliferation in different solid tumor cell lines (A431, 8701-BC, SaOS-2, and PC3).¹⁹ Other members of this family were able to inhibit the proliferation of three Bcr-Abl-positive human leukemia cell lines (K-562, KU-812, and MEG-01), to reduce Bcr-Abl tyrosine phosphorylation and to promote apoptosis of Bcr-Abl-expressing cells.²⁰ Among these inhibitors, a promising antileukemia lead (compound 1, Figure 1) has recently been identified and proven to be active (LD₅₀ range: 0.7–4.3 μM) in Ba/F3 cell lines transducing both the wild type (WT) p210Bcr-Abl construct (IM-sensitive) and three of the most common mutations associated

Table 1. Predicted ADME Properties and Experimental Enzymatic Activities for the Synthesized Compounds



Entry	Compd	R ¹	R ²	R ³	X ^a	Predicted PK properties				K _i (μM) ^f	
						QP-LogP ^b	QP-LogS ^c	QP-LogK ^d	QP-Caco ^e	c-Src	c-Abl
1	1	H	4-F-Bn	4-Cl	A	6.3	-7.6	1.0	3214	0.8±0.1	0.08±0.01
2	18	SCH ₃	Bn	H	A	6.1	-6.6	1	3400	3.7±0.4	0.26±0.03
3	17a	H		4-F	A	4.8	-6.2	0.56	1736	3.0±0.3	1.6±0.2
4	17b	H		4-F	A	5.2	-6.4	0.67	2335	8.3±0.7	2.1±0.1
5	17c	H		4-Cl	A	5.1	-6.6	0.63	1736	3.9±0.3	0.66±0.07
6	17d	H		4-Cl	A	5.4	-6.8	0.74	2385	4.8±0.4	1.2±0.1
7	3a	CH ₃ SO ₂	Bn	H	A	4.4	-6.2	0.42	760	0.74±0.07	2.0±0.2
8	5b	CH ₃ SO ₂	<i>n</i> -Pr	H	B	2.6	-4.8	0.028	595	3.0±0.3	0.72±0.05
9	6c	HO(CH ₂) ₂ NH	phenylethyl	H	B	4.7	-6.5	0.58	590	2.4±0.2	0.22±0.02
10	11	morpholinyl	3-Cl-Ph	H	A	6.0	-7.5	1.25	3950	7.6±0.7	0.39±0.04
11	15a	 N-(CH ₂) ₂ S-	<i>n</i> -Pr	H	A	4.7	-4.7	0.60	770	3.8±0.3	0.34±0.03
12	15b	 N-(CH ₂) ₂ S-	Bn	H	A	5.7	-5.6	0.87	795	2.9±0.3	0.09±0.01
13	15c	 N-(CH ₂) ₂ S-	4-F-Bn	H	A	5.9	-6.0	0.91	795	1.2±0.1	0.58±0.06
14	15d	 N-(CH ₂) ₂ S-	phenylethyl	H	A	6.0	-6.0	0.98	730	NA	0.27±0.03
15	15e	 N-(CH ₂) ₂ S-	3-Cl-Ph	H	A	6.2	-6.4	0.98	795	0.19±0.02	0.12±0.01
16	15f	 N-(CH ₂) ₂ S-	Ph	H	A	5.4	-5.4	0.79	760	0.21±0.02	0.15±0.02
17	Imatinib	-	-	-	-	3.8	-4.8	0.58	93	31.0±3.0	0.013±0.01

^a A = CH₂CHCl; B = CH=CH. ^b Predicted octanol/water partition coefficient; range of recommended values (-2.0)–(+6.5). ^c Predicted aqueous solubility; range of recommended values (-6.5)–(+0.5). ^d Prediction of binding to human serum albumin; range of recommended values (-1.5)–(+1.5). ^e Predicted apparent Caco-2 cell permeability in nm/s; range of recommended values, <25 poor; >500 great. ^f K_i values toward isolated Abl calculated according to the following equation: $K_i = ID_{50} / \{E_0 + [E_0(K_m(ATP)/S_0)]\} / E_0$, where E₀ and S₀ are the enzyme and the ATP concentrations (0.005 and 0.012 μM, respectively).

with IM-resistance in vivo (T315I, Y253F, and E255K).²¹ Unfortunately, the pharmaceutical properties of compound **1** are substandard, mainly due to its low water solubility. Accordingly, the present study describes a lead optimization approach to develop novel analogues of compound **1** as promising antileukemia agents. Molecular modeling studies, previously conducted by us, predicted two different binding modes within Src and Abl for our collection of substituted pyrazolo[3,4-*d*]pyrimidines, depending on the C6-functionalization on the central heterocyclic scaffold.²² Taking into account the above-described docking poses, a series of polar moieties have been introduced on the C4 and C6 water exposed positions of the pyrazolo[3,4-*d*]pyrimidine scaffold

(Table 1), trying to improve the in vitro ADME properties of the compounds while maintaining the dual Src/Abl activity of lead **1**. The compounds showing the best predicted ADME properties were then synthesized and screened in a cell-free assay for their dual Src/Abl activity. The most active inhibitors, representative of the two classes (C4- and C6-substituted derivatives), were then selected for further biological evaluation in different leukemia cell lines (K-562, MEG-01, and KU-812) under normoxic and hypoxic conditions. In vitro ADME properties (PAMPA permeation, water solubility, and metabolic stability) were also experimentally evaluated for the most interesting compounds in order to have a reliable indication of their plasma level after oral administration.

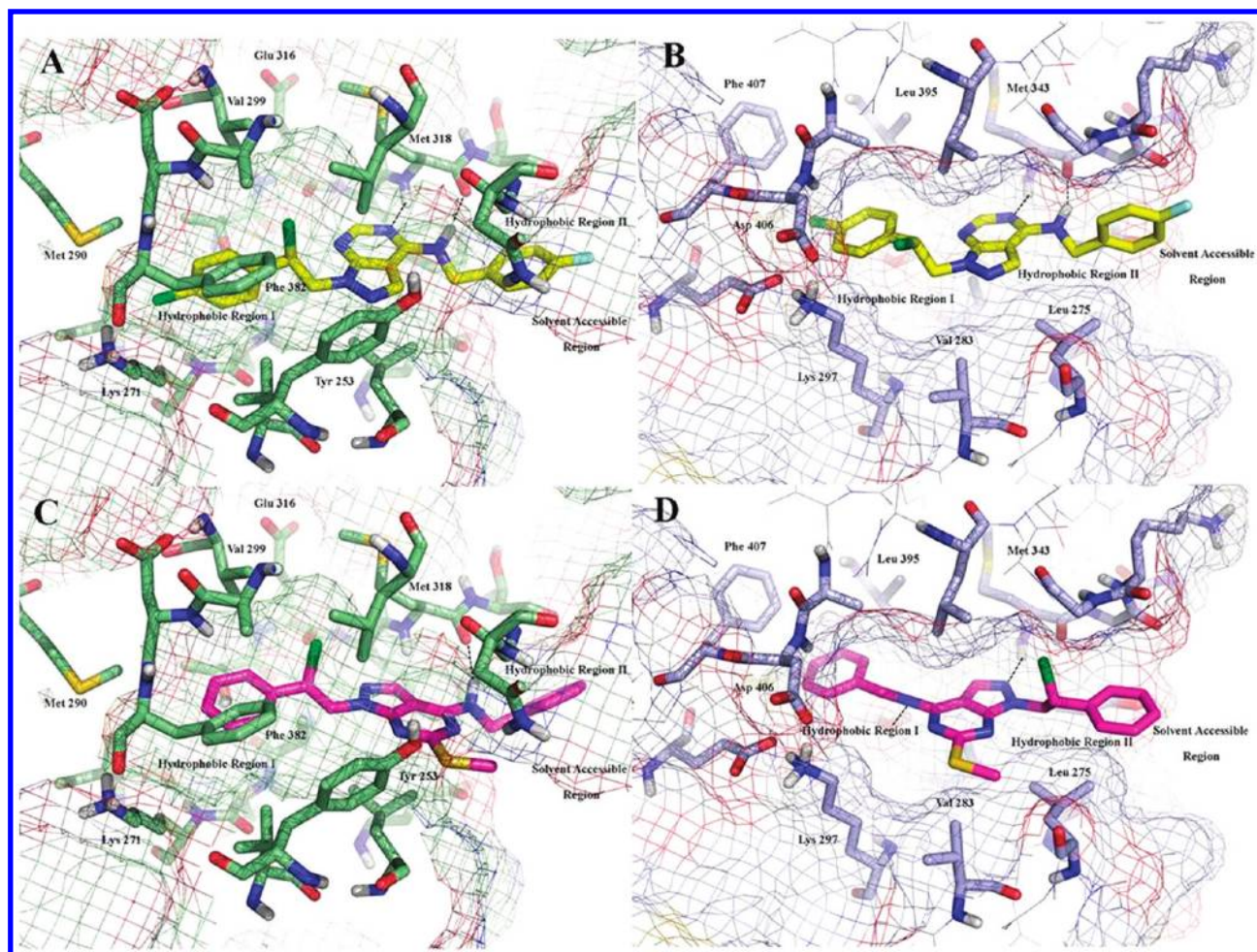


Figure 2. (A) Graphical representation of the binding modes of compound **1** (yellow sticks) into the ATP binding site of Abl (pale green sticks) and (B) Src (light blue sticks). (C) Graphical representation of the binding modes of compound **18** (magenta sticks) into the ATP binding site of Abl (pale green sticks) and (D) Src (light blue sticks). For the sake of clarity, only a few residues are labeled, nonpolar hydrogen atoms are omitted, and hydrogen bond interactions are represented by black dashed lines.

Overall, these efforts led to the discovery of a few compounds characterized by an activity profile similar to that of lead **1** but endowed with better water solubility and permeation and low first-pass metabolism. Finally, the experimental ADME data were integrated with the prediction obtained by the software MetaSite, thus allowing us to propose the most likely sites of metabolism (So-M) of our compounds. This information could guide the design of further improved pyrazolo[3,4-*d*]pyrimidine derivatives as promising antileukemia drugs.

RESULTS AND DISCUSSION

Molecular Modeling. Docking studies recently conducted by our research group on a collection of highly functionalized pyrazolo[3,4-*d*]pyrimidine derivatives highlighted the structural features responsible for their dual Src/Abl inhibitory activity.²² Different binding modes within the ATP pocket of Src and Abl were identified, depending on the functionalization of the C6 position of the pyrazolo[3,4-*d*]pyrimidine ring: as an example, the proposed binding modes for the C6-unsubstituted lead **1** and the closely related C6-substituted derivative **18** are reported in Figure 2. In detail, the C6-unsubstituted derivative **1** binds to both enzymes, positioning the pyrazolo[3,4-*d*]pyrimidine core

within the adenine region, while the side chains at N1 and C4 are directed toward hydrophobic regions I and II, respectively, establishing the classical hydrogen bonds with the hinge region (Met318 in Abl; Met343 in *c*-Src) (Figure 2A,B). However, the C6-substituted derivative **18** showed two different binding modes within the ATP pocket of Src and Abl. In detail, the presence of the C6-substituent induced a reorientation of the pyrazolo[3,4-*d*]pyrimidine nucleus within the Abl binding site, maintaining the N1- and C4-side chains within hydrophobic regions I and II, respectively, and allowing the C6-substituent to interact with hydrophobic region II (Figure 2C). A hydrogen bond interaction was also identified between the C4 amino group and Met318. Within the Src binding pocket, the pyrazolo[3,4-*d*]pyrimidine nucleus of **18** was still accommodated in the adenine region, but the C4 substituent was located in hydrophobic region I, while hydrophobic region II hosted the N1 side chain. Two hydrogen bond interactions were also found, one involving the C4 amino group and the side chain of Thr340 and the other between the N2 of the pyrazolo[3,4-*d*]pyrimidine nucleus and the NH-backbone of Met343 (Figure 2D).

Taking into account the above-described binding modes, we sought to alter the structure of lead **1** in such a way as to maintain the dual Src/Abl activity while improving the pharmaceutical

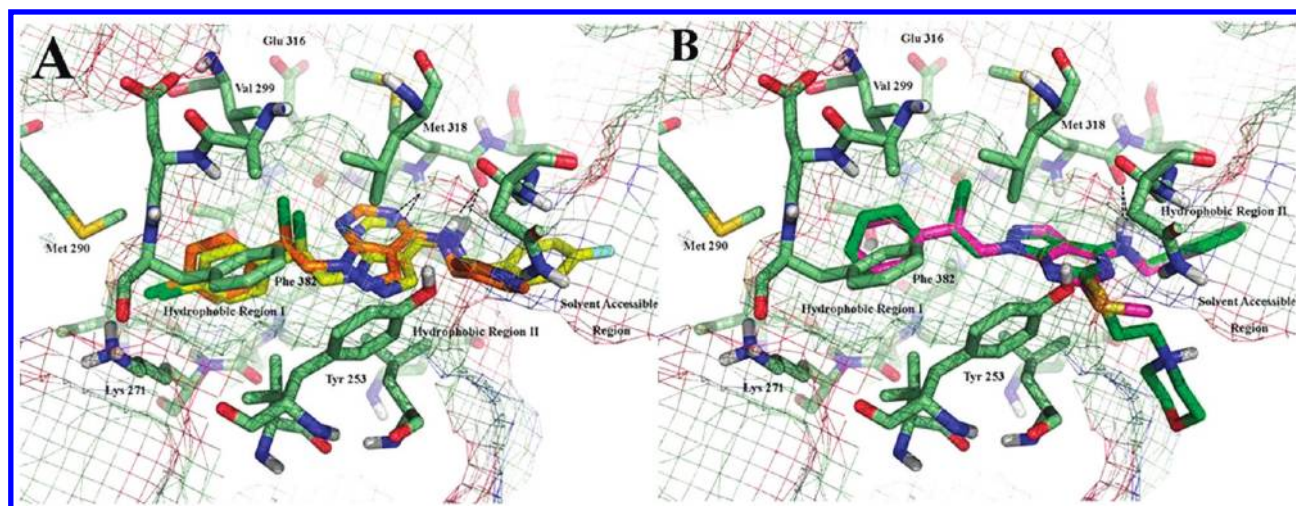
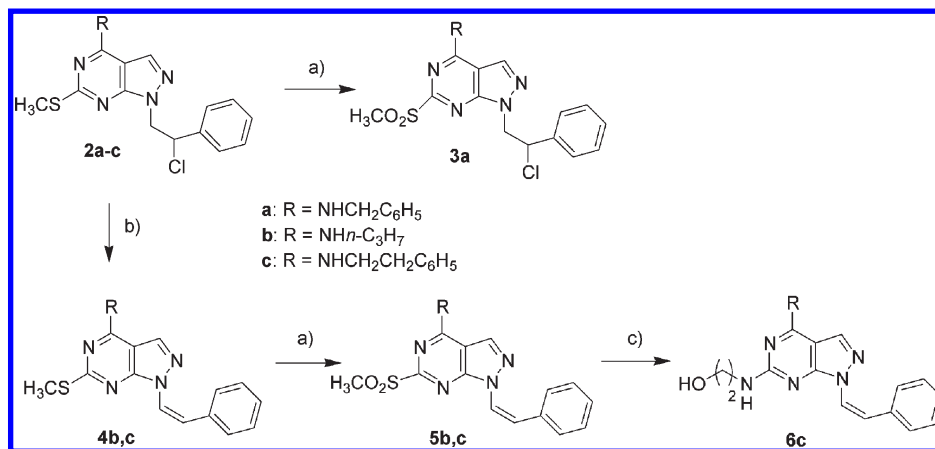


Figure 3. (A) Graphical representation of the binding modes of compound **17c** (orange sticks) and **1** (yellow sticks) into the ATP-binding site of Abl (pale-green sticks). (B) Graphical representation of the binding modes of compound **15b** (green sticks) and **18** (magenta sticks) into the ATP binding site of Abl (pale-green sticks). For the sake of clarity, only a few residues are labeled, nonpolar hydrogen atoms are omitted, and hydrogen bond interactions are represented by black dashed lines.

Scheme 1. Preparation of Pyrazolo[3,4-*d*]pyrimidines Having a Polar Group in C6^a

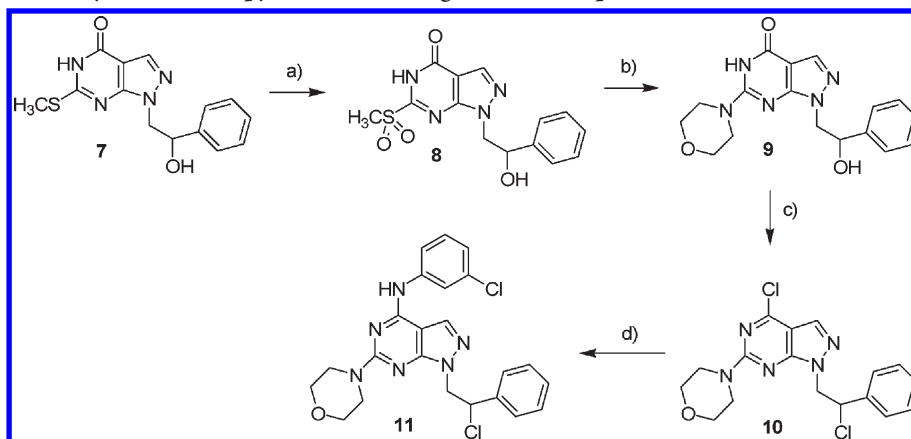


^a Reagents and conditions: a) 3-chloroperoxybenzoic acid, CHCl_3 , r.t., 6 h; b) NaOH, EtOH, reflux, 5 h; c) 2-aminoethanol, DMSO, butan-1-ol, 90°C , 12 h.

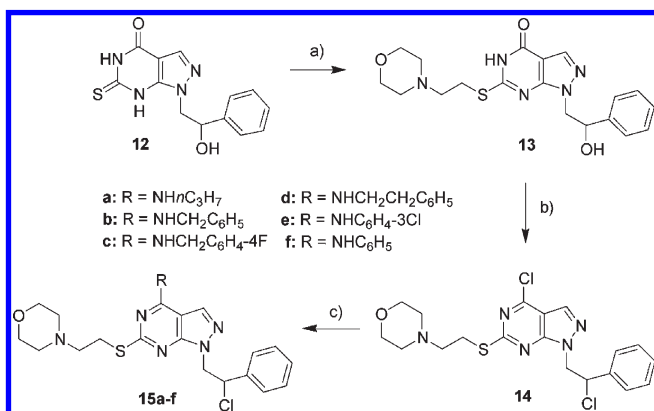
properties: a series of analogues, predicted as more water-soluble, were thus designed by introducing different polar moieties in the solvent-exposed C4 and C6 positions of the pyrazolo[3,4-*d*]pyrimidine scaffold. The virtual library of compounds, designed by combining the opportune substituents in N1, C4, and C6, was docked within the ATP pocket of Src and Abl: as a result, only those derivatives showing better predicted activity and ADME properties with respect to lead **1** were selected for the next synthesis (see Table 1). The predicted ADME properties have been calculated using the QikProp 2.5 protocol, implemented in Maestro8.5,²³ and the results obtained were compared with those of the reference compounds **1**, **18**, and IM. In particular, four descriptors were determined and analyzed: QP-LogP, QP-LogS, QP-LogK, and QP-Caco (Table 1). All the new compounds were predicted to have a great Caco-2 cell permeability (QP-Caco values larger than 500) and a better aqueous solubility with respect to lead compound **1** (QP-LogS between -4.7 and -7.5). Concerning the lipophilicity of the selected compounds, the predicted octanol/water partition coefficient

(QP-LogP) was lower than that of lead **1**, while the predicted binding to human serum proteins (QP-LogK) fell in the range of recommended values. In detail, compounds **17a–d** were characterized by the presence of a polar 4-picolyl or a 2-picolyl moiety bound to the C4-amino group: these substituents can in fact be considered as more soluble bioisosters of the fluoro-phenyl ring characteristic of the lead and were predicted to have better ADME properties than **1** and additional polar contacts in the solvent accessible region. A representative example is reported in Figure 3A: the 4-picolyl-derivative **17c** docked within Abl showed a binding mode highly superimposable to that of lead **1**, with the picolyl group located in the solvent-exposed portion of the hydrophobic region II and giving a weak hydrogen bond interaction with Asn322.

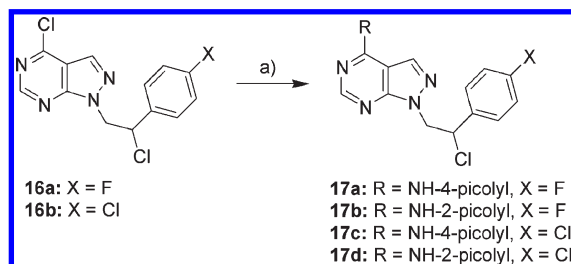
However, compounds bearing a polar moiety in C6 were all characterized by the typical binding mode previously described for the other C6-substituted derivatives, and the polar group seems to influence only the ADME properties of the designed derivatives with a general improvement in comparison with the

Scheme 2. Preparation of Pyrazolo[3,4-*d*]pyrimidines Having a Polar Group in C6^a

^a Reagents and conditions: (a) 3-chloroperoxybenzoic acid, CHCl_3 , r.t., 12 h; (b) morpholine, DMSO, 100 °C, 3 h; (c) POCl_3/DMF , CHCl_3 , reflux, 12 h; (d) 3-chloroaniline, abs. EtOH, reflux, 5 h.

Scheme 3. Preparation of Pyrazolo[3,4-*d*]pyrimidines Having a Polar Group in C6^a

^a Reagents and conditions: (a) 4-(2-chloroethyl)morpholine, NaOH, EtOH, DMF, reflux, 6 h; (b) POCl_3/DMF , CHCl_3 , reflux, 8 h; (c) method A, amine, toluene, r.t., 24 h; method B, aniline, abs. EtOH, reflux, 3–5 h.

Scheme 4. Preparation of Pyrazolo[3,4-*d*]pyrimidines Having a Polar Group in C4^a

^a Reagents and conditions: (a) RNH_2 , AcOH, dioxane, 150 °C, μW 10 min.

reference compounds **1** and **18** (Table 1, entries 7–16). As an example, compound **15b** showed the same key interactions of **18** within the catalytic site of Abl, while, as expected, the C6-substituent of **15b** seemed to occupy the solvent-accessible region (Figure 3B).

Chemistry. Compounds bearing a polar moiety in C6 (Table 1, entries 7–16) were synthesized as reported in Schemes 1–3. Compound **3a** was prepared starting from compound **2a**, previously reported by us,^{19a} by oxidation of the methylthio group in C6 with 3-chloroperoxybenzoic acid in CHCl_3 (Scheme 1). Compounds **5b** and **6c** were synthesized starting from **2b,c**, which were initially dehydrohalogenated by refluxing with NaOH to give the corresponding N1-unsaturated derivatives **4b,c**. Oxidation of the latter intermediates with 3-chloroperoxybenzoic acid in CHCl_3 gave the 6-methylsulfonyl derivatives **5b,c**. Finally, compound **6c** was obtained by nucleophilic substitution of the methylsulfonyl group with 2-aminoethanol in dimethylsulfoxide (DMSO) at 90 °C for 12 h in good yield.

The synthesis of compound **11** is reported in Scheme 2. Starting from the intermediate **7**,^{19a} oxidation with 3-chloroperoxybenzoic acid in CHCl_3 at room temperature afforded the corresponding 6-methylsulfonyl derivative **8** in good yield (57%). The latter intermediate was treated with an excess of morpholine in DMSO at 100 °C for 3 h to give 1-(2-hydroxy-2-phenylethyl)-6-morpholin-4-yl-1,5-dihydro-4H-pyrazolo[3,4-*d*]pyrimidin-4-one **9**, which was in turn treated with the Vilsmeier complex (POCl_3/DMF) in CHCl_3 to obtain the dihalogenated compound **10**. Reaction of **10** with a little excess of 3-chloroaniline in absolute ethanol gave the desired compound **11**.

Synthesis of compounds **15a–f** is reported in Scheme 3. Alkylation of the C6 thiocarbonyl group of the intermediate **12**^{19a} with 4-(2-chloroethyl)morpholine gave the 6-(2-morpholin-4-ylethylthio) derivative **13**, which was in turn treated with the Vilsmeier complex (POCl_3/DMF) in CHCl_3 at reflux for 8 h to obtain the dihalogenated compound **14** in good yield (75%). Finally, the reaction of **14** with an excess of the appropriate amine in toluene at room temperature afforded compounds **15a–d** in yields ranging from 60 to 70%. Differently, the aniline derivatives **15e,f** were obtained by a reaction of **14** with the appropriate aniline in absolute ethanol at reflux for 3–5 h.

Synthesis of compounds bearing a polar moiety in C4 (**17a–d**) is reported in Scheme 4. The synthesis of the substrates **16a,b** has already been reported by us.^{22c} A microwave-assisted procedure has been developed to accelerate the introduction of the appropriate amine in C4, which usually requires a long reaction time under standard conditions. Accordingly, treating

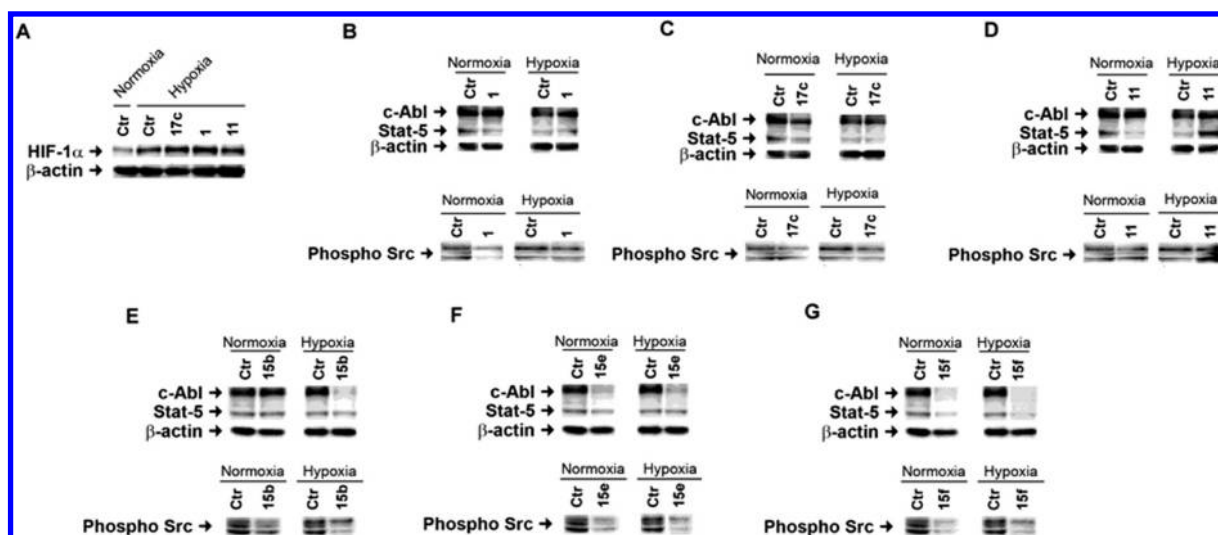


Figure 4. Antiproliferative properties of selected compounds (50 μ M) both in normoxic and in hypoxic conditions. (A) The effect of compounds 17c, 1, and 11 on the expression of HIF-1 α in hypoxic condition was analyzed by Western blot. (B–D) The effects of compounds 1 (panel B), 17c (panel C), 11 (panel D), 15b (panel E), 15e (panel F), and 15f (panel G) on the phosphorylation of c-Abl, STAT-5, and Src in K-562 cells in normoxia and hypoxia, after 3 h of treatment, were detected using specific antibodies. Anti- β -actin antibody was used as the protein loading control. The membranes were visualized with luminescent substrates. The figure is a representative gel of three similar experiments.

compounds **16a,b** with 1.5 equiv of the appropriate amine and 1.5 equiv of acetic acid in dioxane at 150 $^{\circ}$ C under microwave irradiation afforded compounds **17a–d** in yields ranging from 50 to 70% after only 10 min.²⁴

Biology. The synthesized compounds were initially tested in a cell-free assay to evaluate their affinity toward Src and Abl enzymes in comparison with IM (see Table 1): all the compounds, with the exception of **15d**, maintained the dual Src/Abl inhibitory profile of lead **1**, while generally showing an improvement of the predicted ADME properties (as described in the previous section). In particular, an inverse relationship between the bulkiness of the C4 substituent (R_2) and Src inhibitory activity was found for the most interesting compounds **15b,c,e,f**: the C4-anilino derivatives **15e,f** were the most active ($K_i = 0.19$ and 0.21μ M, respectively), and the C4-benzylamino derivatives **15b,c** showed decreased activity ($K_i = 2.9$ and 1.2μ M, respectively), while the C4-phenylethyl derivative **15d** was completely inactive. Although these compounds showed Abl inhibitory activity comparable to that of lead **1**, compounds **15e,f** proved to be more effective than **1** as dual Src/Abl inhibitors.

The most interesting compounds, representative of the two classes of inhibitors (C4- and C6-substituted derivatives), were then evaluated for their antiproliferative activity on three human leukemia cell lines (K-562, MEG-01, and KU-812) using lead **1** as a reference (Table 2). These compounds showed antiproliferative activity toward the three cell lines in the range from low-micromolar to micromolar concentration, and all the cell lines seemed to be equally sensitive to the treatment with the inhibitors in normoxic conditions. Compounds **1**, **6c**, **11**, **15b**, and **17c** showed the best biological profile in terms of antiproliferative activity in normoxic conditions and were therefore selected to test their antiproliferative activity toward leukemic cells also in hypoxic conditions.

Hypoxia is an important environmental factor to be considered in the biological investigation of potential antileukemia agents because bone marrow is intrinsically hypoxic in nature.²⁵ Hypoxia is known to be associated with both radio- and chemo-resistance in solid tumors, but its role in leukemia has been poorly investigated,

particularly in the context of resistance to targeted therapies. Preliminary investigations on the role of hypoxia in leukemia and IM-resistance showed that low oxygen concentration suppresses Bcr-Abl expression and phosphorylation, conferring complete IM-resistance.¹⁶ It has also been recently reported that human Bcr-Abl(+) cells engrafted in the bone marrow of immunodeficient mice survive under severe hypoxia and that hypoxia-adapted Bcr-Abl(+) cell lines exhibit stem cell-like characteristics, including resistance to Abl TKIs and higher transplantation efficiency.²⁶ Hypoxic adaptation is mainly provided by hypoxia-inducible factor-1 (HIF-1), which orchestrates cellular adaptation to hypoxia by transactivating about 100 genes.²⁷

In order to explore the effect of hypoxia on the activity of the selected compounds, the three cell lines were cultured at 2% O₂, and, as expected, HIF-1 α expression was significantly increased after 3 h of incubation.²⁸ We initially explored the effect of **1**, **11**, and **17c** on HIF-1 α expression on K-562 cells, but they did not show any influence on HIF-1 α accumulation (Figure 4A). To further understand the mechanism of action of these compounds, we decided to evaluate the phosphorylation of signal transducer and activator of transcription 5 (STAT-5), a transcription factor downstream of Bcr-Abl directly activating Bcl-xL that works as an apoptosis inhibitor at the mitochondrial level, in addition to the phosphorylation of Src. Previous studies with Src dominant-negative mutants suggested in fact that Src kinases play a role in the proliferation of Bcr-Abl expressing cell lines and that overexpression of Src kinases is implicated in Bcr-Abl-mediated leukemogenesis and in IM-resistance.²⁹ As a result, compound **1** markedly reduced Src and STAT-5 phosphorylation on K-562 cells with respect to control both in normoxic and hypoxic conditions (Figure 4B). On the same cell line, **17c** reduced Src phosphorylation with respect to the control and showed an increased effect in hypoxic conditions. STAT-5 phosphorylation was almost abolished in hypoxic conditions and significantly reduced in normoxia (Figure 4C). On the same line of action was compound **15b**, which also showed a better effect on the reduction of c-Abl phosphorylation in hypoxic conditions with

respect to the normoxic conditions (Figure 4E). Of great interest were the results obtained with compounds **15e** and **15f**: these derivatives were in fact able to almost abolish the phosphorylation of c-Abl, STAT-5 and Src in both experimental conditions (Figure 4F and G). However, compound **11** showed less pronounced activity against both STAT-5 and Src phosphorylation (Figure 4D). The same results were obtained on the other cell lines for all the selected compounds (data not shown).

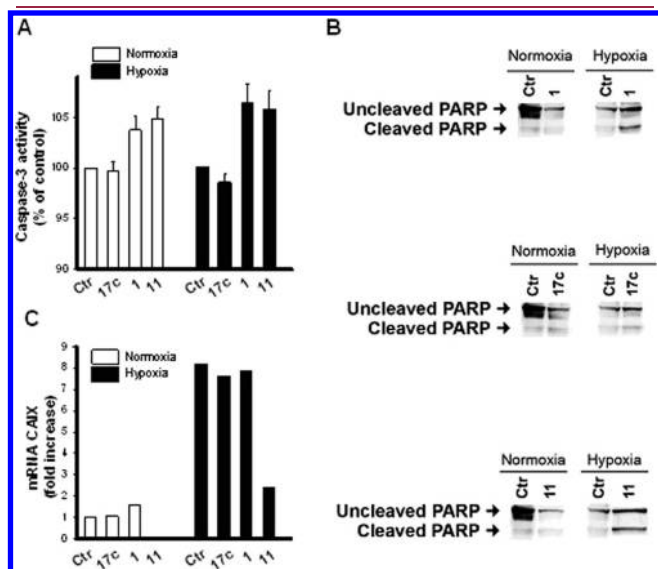


Figure 5. Proapoptotic effect of compounds **1**, **11**, and **17c** both in normoxic and hypoxic conditions. (A) Caspase-3 activity in K-562 cells treated with compounds **17c**, **1**, and **11** in normoxia and hypoxia. (B) Detection of cleaved PARP in K-562 cell extracts. Immunoblot analysis was performed using anti-PARP specific antibodies. An antirabbit secondary antibody conjugated with peroxidase and a peroxidase substrate revealed the presence of PARP cleavage products in apoptotic cells. The antibody recognized both the uncleaved PARP (116 kD) and the larger cleaved fragment (85 kD). (C) CA IX mRNA expression was examined by qRT-PCR after treatment of K-562 cells with compounds **17c**, **1**, and **11** in normoxic and hypoxic conditions. Cells were treated for 72 h with 10 μM of the specified compound. Results are representative of three independent experiments.

The reduction of STAT-5 phosphorylation levels mediated by the inhibitors strongly suggested that the effects on proliferation and apoptosis of leukemia cells are a consequence of the inhibition of Bcr-Abl kinase activity. Moreover, inhibition of STAT-5 phosphorylation caused by our compounds and the involvement of STAT-5 in apoptosis control via Bcl-xL suggested that we should investigate the proapoptotic effect for some selected compounds. Knowing that the sequential activation of caspases plays a central role in the execution phase of cell apoptosis, we analyzed caspase-3 activity, which catalyzes the cleavage of poly-ADP-ribose-polymerase (PARP): compounds **1** and **11** showed higher induction of caspase-3 both in normoxic and hypoxic conditions (Figure 5A). Accordingly, the effect of the compounds on PARP degradation was investigated: the proapoptotic activity of **1**, **11**, and **17c** on K-562 cells was tested using a PARP assay (Roche Diagnostics, Milano, Italy). Immunoblot analysis of uncleaved and cleaved PARP after 72 h of treatment with the specified compounds evidenced a significant increase of the cleaved PARP, which was even more evident in hypoxic conditions for **1** and **11** (Figure 5B). Enhancement of the cleaved PARP level demonstrated that cells were induced in apoptosis. In particular, compounds **1** and **11** showed a proapoptotic effect in hypoxic conditions toward K-562 cells. Despite its significant antiproliferative activity, compound **17c** showed less intense proapoptotic activity; this might be interpreted as a more pronounced cytostatic effect rather than proapoptotic activity. However, it should also be considered that the time of cellular exposure to the compounds might be relevant for apoptotic induction.

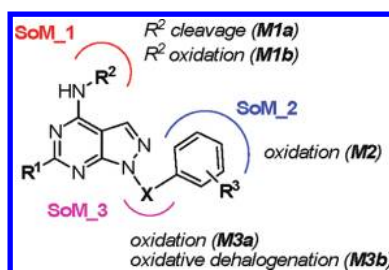
The functional contribution of CAs to hypoxic tumor growth and progression has long been hypothesized, and a number of studies evidenced that CAs are key pro-survival enzymes during tumor hypoxia. Carbonic anhydrases (CA) are zinc metalloenzymes that catalyze the reversible hydration of CO_2 to form HCO_3^- . In particular, CA IX (previously called MN) is related to cell proliferation and oncogenesis,³⁰ is a major downstream target of HIF-1 α , and is overexpressed in a wide spectrum of human cancers, including breast cancer and nonsmall cell lung cancer, but not in normal tissue.³¹ The significant inhibition of expression of CA IX shown in Figure 5C could explain the effect of compound **11** despite its reduced effect on STAT-5 and Src inhibition.

Table 2. Antiproliferative Activity of Selected Compounds Towards K-562, MEG-01, and KU-812 Cell Lines Both in Normoxic and Hypoxic Conditions

entry	compound	IC_{50} (μM) ^a normoxia			IC_{50} (μM) ^a hypoxia		
		K-562	MEG-01	KU-812	K-562	MEG-01	KU-812
1	1 ^b	9.2 \pm 1.9	6.2 \pm 0.4	8.1 \pm 0.8	2.8 \pm 0.2	6.1 \pm 2.4	13.3 \pm 4.7
2	17a	36.5 \pm 4.4	37.4 \pm 5.5	56.4 \pm 5.4	nd ^c	nd	nd
3	17b	37.5 \pm 4.3	23.8 \pm 10.1	40.6 \pm 9.0	nd	nd	nd
4	17c	12.7 \pm 1.3	14.6 \pm 2.6	10.1 \pm 9.8	20.4 \pm 2.3	43.5 \pm 9.0	>100
5	17d	30.6 \pm 2.5	16.6 \pm 3.6	31.4 \pm 0.1	nd	nd	nd
6	11	12.2 \pm 3.1	7.7 \pm 1.2	2.2 \pm 6.5	4.6 \pm 0.1	15.0 \pm 5.3	16.1 \pm 4.9
7	3a	35.8 \pm 2.1	41.4 \pm 7.8	36.1 \pm 2.4	nd	nd	nd
8	6c	2.3 \pm 0.7	12.9 \pm 2.9	nd	8.1 \pm 2.9	34.0 \pm 7.4	nd
9	15b	3.1 \pm 0.7	23.7 \pm 1.6	nd	5.1 \pm 0.8	19.7 \pm 5.8	nd
10	15e	4.5 \pm 0.2	6.1 \pm 1.2	nd	nd	nd	nd
11	15f	2.2 \pm 0.3	nd	nd	4.7 \pm 0.4	nd	nd

^a IC_{50} values are the means \pm SEM of a series separate assays, each performed in triplicate. ^bUsed as the reference compound. ^cnd = not determined.

Table 3. *In Vitro* ADME Properties of Selected Compounds 17c, 11, 15b, 15e, 15f, 6c, 19, and 20 compared to Those of Lead 1 (Representative *in Silico* ADME Properties Are Also Reported)



Entry	Cpd	R ¹	R ²	R ³	X ^a	QP-LogP ^b	QP-Caco ^c	PAMPA ^d Papp × 10 ⁻⁶ (cm/s)	Solub. at pH 7.4 (μg/mL)	Metab. Stability ^e (%)	Major Metabolites ^{f,g} (%)
1	1	H	4-F-Bn	4-Cl	A	6.3	3219	16.6	<0.04	94	M1a = M-R ² (2) M3b = M-HCl+O (4)
2	17c	H		4-Cl	A	5.1	1736	5.4	12.3	90	M1a = M-R ² (5) M1b = M+O (5)
3	11	morpholinyl	3-Cl-Ph	H	A	6	3950	14.8	0.13	90	M2 = M+16 (1) M3b = M-HCl+O (9)
4	15b		Bn	H	A	5.7	795	9.1	1.2	95	M3b = M-HCl+O (5)
5	15e		3-Cl-Ph	H	A	6.2	795	9.5	0.1	95	M3b = M-HCl+O (5)
6	15f		Ph	H	A	5.4	760	10.0	1.7	95	M3b = M-HCl+O (5)
7	6c	HO(CH ₂) ₂ NH	Ph(CH ₂) ₂	H	B	4.7	590	2.6	0.4	84	M1a = M-R ² (9) M2 = M+O (3) M3a = M+O (2) ^h M3a = M+O (2) ^h
8	19	H	3-Cl-Ph	H	C	5.4	3772	13.5	<0.04	75	M2 = M+O (20) M3a = M+O (5)
9	20	H	4-F-Bn	4-F	A	6.0	3647	11.0	<0.04	82	M1a = M-R ² (2) M3b = M-HCl+O (16)

^a A = CH₂CHCl; B = CH=CH; C = CH₂CHMe. ^b Predicted octanol/water partition coefficient; range of recommended values (−2.0)–(+6.5). ^c Predicted apparent Caco-2 cell permeability (in nm/s); range of recommended values <25 poor; >500 great. ^d PAMPA see Experimental Section for details. ^e Expressed as the percentage of unmodified parent drug. ^f M = mass of the parent drug; M1–3 = experimental mass of the identified metabolites (the numbers correspond to the proposed sites of metabolism, as indicated in the above general structure); the percentage of each single metabolite experimentally determined via LC-MS is reported in parentheses. ^g The structure of the metabolites predicted by Metasite is reported in Table S2 of the Supporting Information. ^h The two oxidized metabolites M3a are predicted by Metasite to be an epoxide and the ketone; see Table S2, Supporting Information for details.

In Vitro ADME Study. In recent years, there has been considerable discussion on the importance of optimizing the absorption, distribution, metabolism, and excretion (ADME) properties of drug candidates, in addition to their efficacy, to increase the rate of drug discovery successes and to advance high quality candidates to clinical studies. Early property assessment and optimization provide the opportunity for earlier correction of property limitations, thus reducing the risk of drug failure in advanced phases. In this regard, a few *in vitro* experiments can be easily conducted to quickly establish the absorption/stability of drug candidates in an early phase: aqueous solubility, parallel artificial membrane permeability assay (PAMPA), and human liver microsome (HLM) stability determination.³² These experiments have in fact proven to be reliable indicators of plasma exposure level after oral administration.³³ Accordingly, the most

active compounds previously identified (1, 17c, 11, 15b, 15e, 15f, 6c) were submitted to a thorough ADME study to identify among them promising drug candidates endowed with better water solubility and permeation and low first-pass metabolism (Table 3). Compounds 19³⁴ and 20^{22c} (Table 3, entries 8–9), having a different functionalization on the N1 side chain, were also analyzed in this part of the study to get a bigger picture of the ADME properties of the pyrazolo[3,4-*d*]pyrimidine family. Results of the *in vitro* ADME study are reported in Table 3.

Passive membrane permeability has been initially evaluated with the PAMPA assay applying a validated protocol recently developed by us for poor water-soluble pyrazolo[3,4-*d*]pyrimidine:³⁵ although the presence of a cosolvent (DMSO) proved to slightly decrease the permeability of the compounds, a good correlation was found with the experimental data, and overall,

this protocol gives useful insights in ranking the intestinal absorption of lipophilic compounds. The solubility of compounds **1**, **17c**, **11**, **15b**, **15e**, **15f**, **6c**, **19**, and **20** was then evaluated following the method developed by Avdeef et al.,³⁶ and results were expressed in $\mu\text{g/mL}$. Metabolic stability was finally evaluated by incubating the above-mentioned compounds with $5\ \mu\text{L}$ of man-pooled HLM for 1 h at $37\ ^\circ\text{C}$ in order to simulate first-pass metabolism. The parent drugs and metabolites were subsequently determined by LC-MS analysis (see Experimental Section for details). The metabolic stability reported in Table 3 is expressed as the percentage of the unmodified parent drug remaining in the mixture, while the different metabolites (M1–M3 in Table 3) were separated in HPLC and analyzed via mass spectrometry. The information on the metabolites' mass obtained with the latter spectroscopic studies was then integrated with the *in silico* metabolites' prediction obtained with the software MetaSite³⁷ (predicted metabolites are reported in the Supporting Information, Table S2), thus allowing us to propose likely sites of metabolism (SoM_1–3, Table 3). However, while most of the experimental metabolites were predicted by MetaSite, M3b was never identified by the software as a possible metabolite. This could have resulted from a less common P450-catalyzed metabolic reaction (an oxidative dehalogenation on the linker X). A clear understanding of the metabolic transformations for this class of compounds could give useful insights for their further optimization and for the implementation of the software MetaSite. Accordingly, a thorough study on the characterization of each single product of the P450-mediated metabolic transformation is currently ongoing and will be reported in due course.

The interpretation of the ADME data and their translation into optimized drug candidates also requires an understanding of the structure–metabolism relationship (SMR) and the accurate identification of the soft spots of the molecules to design novel compounds with improved PK profiles. Overall, the ADME investigation on our pyrazolopyrimidine derivatives highlighted good metabolic stability (ranging from 75 to 95%) and membrane permeability (ranging from 2.6 to $16.6 \times 10^{-6}\ \text{cm/s}$) for most of the tested compounds and an enhanced water solubility, especially for compounds **17c**, **15b**, and **15f** (12.3, 1.2, and $1.7\ \mu\text{g/mL}$, respectively). The combination of MetaSite predictions and experimental data from microsomal assays allowed us to propose three main soft spots for our family of inhibitors: (1) the C4-substituent (NHR²); (2) the linker X on N1; and (3) the substituted phenyl (R³-Ph) on N1. It was interesting to note that the C6-substituent (R¹) was not the subject of any metabolic reaction (e.g., N or S oxidation), and therefore, the functionalization of this position with polar groups to improve the solubility of lead **1** (as we did with compounds **3a**, **4b**, **6c**, **11**, and **15a–f**) can be considered as the best possible solution to improve the ADME properties of this family of compounds.

In detail, compound **11** showed values of membrane permeation and metabolic stability comparable to that of lead **1** but suffered from low aqueous solubility, and **6c** showed low permeation, low solubility, and poor stability, giving four different metabolites after incubation with human microsomes (Table 3, entries 3 and 7). Even if the benzylic chlorine on the N1-linker (X = A) could be considered as the most likely site of metabolism for our molecules, it underwent less common P450-mediated oxidative dehalogenation, giving the corresponding metabolite M3b only in low percentages. To our surprise, it was interesting to note that the replacement of this chlorine with a methyl group (X = C, Table 3, entry 8) afforded the less stable

compound **19**, which was more sensitive to P450-mediated oxidation on the N1-substituent. The functionalization of the aromatic ring in N1 also proved to play an important role in the metabolism rate: replacing a chloro with a fluoro in R³ (compounds **1** and **20**, respectively) considerably increased the amount of the corresponding metabolite M3b from 4 to 16% (Table 3, entries 1 and 9). Among the tested compounds, **17c** and **15b,f** were finally identified as the most promising derivatives, showing values of membrane permeation and metabolic stability comparable to that of lead **1** but presenting with much improved aqueous solubility profiles (Table 3, entries 2, 4, and 6). The latter compounds showed an activity profile comparable to that of **1**, with dual Src/Abl activity in the nanomolar/low-micromolar range and micromolar/low-micromolar antiproliferative activity in three different leukemic cell lines (K-562, MEG-01, and KU-812) in both normoxic and hypoxic conditions. Compounds **17c** and **15b,f** can therefore be considered as improved analogues of lead **1**, showing, at the same time, a profitable balance of different ADME properties (permeation, water solubility, and metabolic stability) and a promising biological profile also on hypoxic leukemic cells that are generally resistant to TKIs.

Conclusions. In summary, among the pyrazolo[3,4-*d*]pyrimidines developed so far by our research group as antitumor agents, a promising antileukemia lead (**1**) has been recently identified, but, unfortunately, it suffered from substandard pharmaceutical properties. In the present study, a series of optimized analogues rationally designed by introducing different polar moieties in the C4 and C6 solvent exposed positions of the pyrazolo[3,4-*d*]pyrimidine scaffold were prepared. Biological evaluation showed dual Src/Abl activity similar to that of the lead **1** for most of the synthesized compounds and promising antiproliferative activity in three different leukemic cell lines (K-562, MEG-01, and KU-812) both in normoxic and in hypoxic conditions. Finally, *in vitro* ADME properties (permeation, water solubility, and metabolic stability) and metabolic soft spots for the synthesized compounds were also determined, allowing us to identify compounds **17c** and **15b,f** as optimized analogues of lead **1**. Compounds **17c** and **15b,f** showed, at the same time, a profitable balance of different ADME properties and biological activity in leukemia cells. Interestingly, these compounds also resulted active in hypoxic leukemic cells that are generally resistant to TKIs. Further investigations on these advanced leads are ongoing and will be reported in due course.

EXPERIMENTAL SECTION

Molecular Modeling. Docking studies were performed by means of the software Gold, version 4.1,³⁸ which uses a genetic algorithm (GA) to explore the conformation/orientation space. For each of the 50 independent GA runs, a maximum number of 100,000 GA operations were performed on a set of five groups with a population size of 200 individuals; the other GA parameters not mentioned herein were set to default values. Hydrophobic fitting points were calculated on the target for a 5 Å radius around the cocrystallized ligand. Chemscore was used as the scoring function. For each ligand, the first ranked solution was selected for further analysis. Structures of inhibitors were represented using MacroModel 8.5³⁹ and processed with the Schrödinger LigPrep tool to obtain the protonation state of each compound at physiological pH. A preliminary structure minimization was performed with MacroModel 8.5 on the X-ray crystallographic structure of both c-Abl and c-Src (entry 1M52)⁴⁰ and 1YOL⁴¹ on the Brookhaven Protein Data Bank

through the all-atom Amber* force field and the Polak-Ribiere conjugate gradient method. 1YOL missing loops were completed before minimization by superimposition with the 1Y57 X-ray structure.⁴² A continuum solvation method, with water as the solvent, was also applied. Extended cut-offs were used, and convergence was set to 0.01 kJ/mol·Å.

Chemistry. Starting materials were purchased from Aldrich-Italia (Milan, Italy). Melting points were determined with a Büchi 530 apparatus and are uncorrected. IR spectra were measured in KBr with a Perkin-Elmer 398 spectrophotometer. ¹H NMR spectra were recorded in a (CD₃)₂SO solution on a Varian Gemini 200 (200 MHz) instrument. Chemical shifts are reported as δ (ppm) relative to TMS as the internal standard, *J* in Hz. ¹H patterns are described using the following abbreviations: s = singlet, d = doublet, t = triplet, q = quartet, quint = quintet, sx = sextet, m = multiplet, and br = broad. TLC was carried out using Merck TLC plates silica gel 60 F254. Chromatographic purifications were performed on columns packed with Merck 60 silica gel, 23–400 mesh, for flash technique. Analyses for C, H, N, and S were within ±0.3% of the theoretical value. Mass spectra (MS) data were obtained using an Agilent 1100 LC/MSD VL system (G1946C) with a 0.4 mL/min flow rate using a binary solvent system of 95:5 methanol/water. UV detection was monitored at 254 nm. MS were acquired in positive and negative modes, scanning over the mass range 50–1500. The following ion source parameters were used: drying gas flow, 9 mL/min; nebulizer pressure, 40 psig; drying gas temperature, 350 °C. All target compounds possessed a purity of ≥95% as verified by elemental analyses by comparison with the theoretical values.

Microwave Irradiation Experiments. Microwave irradiation experiments were conducted using a CEM Discover Synthesis Unit (CEM Corp., Matthews, NC). The machine consists of a continuous focused microwave power delivery system with operator-selectable power output from 0 to 300 W. The temperature of the contents of the vessels was monitored using a calibrated infrared temperature control mounted under the reaction vessel. All the experiments were performed using a stirring option whereby the contents of the vessel are stirred by means of a rotating magnetic plate located below the floor of the microwave cavity and a Teflon-coated magnetic stir bar in the vessel.

Synthesis and analytical data of compounds **2a**, **2b**, **2c**, **4c**, **7**, and **12**,¹⁹ and **16a**, **16b**, and **20**^{22c} were previously reported by us.

Synthesis of *N*-Benzyl-1-(2-chloro-2-phenylethyl)-6-(methylsulfonyl)-1*H*-pyrazolo[3,4-*d*]pyrimidin-4-amine (3a**).** 3-Chloroperoxybenzoic acid (2 mmol, 0.5 g of 77% suspension in mineral oil) was added portion wise to a solution of *N*-benzyl-1-(2-chloro-2-phenylethyl)-6-(methylthio)-1*H*-pyrazolo[3,4-*d*]pyrimidin-4-amine **2a** (0.41 g, 1 mmol) in CHCl₃ (10 mL) at 0 °C. The mixture was stirred at room temperature for 6 h; the organic phase was washed with saturated NaHCO₃ solution (2 × 20 mL), then with water (20 mL), dried (MgSO₄), and evaporated under reduced pressure. The crude was crystallized by adding petroleum ether (40–60 °C); the pale yellow solid was recrystallized from absolute ethanol (0.20 g, 46%). Mp: 169–170 °C. ¹H NMR: δ 3.21 (s, 3H, SO₂CH₃), 4.64–4.96 (m, 4H, CH₂N + CH₂Ar), 5.34–5.44 (m, 1H, CHCl), 6.44 (br s, 1H, NH disappears with D₂O), 7.14–7.38 (m, 10H Ar), 7.99 (s, 1H, H-3). IR cm⁻¹: 3308 (NH), 1301, 1132 (SO₂). MS: *m/z* 442 [M+1]⁺. Anal. (C₂₁H₂₀N₅O₂ClS) C, H, N, S.

Synthesis of 6-(Methylthio)-1-(2-phenylvinyl)-*N*-propyl-1*H*-pyrazolo[3,4-*d*]pyrimidin-4-amine (4b**).** A solution of NaOH (0.3 g, 7.5 mmol) in water (2.15 mL) was added to a suspension of 1-(2-chloro-2-phenylethyl)-6-(methylthio)-*N*-propyl-1*H*-pyrazolo[3,4-*d*]pyrimidin-4-amine **2b** (0.36 g, 1 mmol), in 95% ethanol (12 mL), and the mixture was refluxed for 5 h. After cooling, the white solid was filtered, washed with water, and recrystallized from absolute ethanol (0.26 g, 80%). Mp: 180–181 °C. ¹H NMR: δ 1.07 (t, *J* = 7.4, 3H, CH₃), 1.75 (sx, *J* = 7.4, 2H, CH₂CH₃), 2.65 (s, 3H, SCH₃), 3.60 (q, *J* = 7.4, 2H, CH₂NH), 5.44 (br s, 1H, NH disappears with D₂O), 7.21–7.54 (m, 6H, 5H Ar + CH=), 7.95 (s, 1H, H-3), 7.98 (d, *J*_{trans} = 14.0, 1H,

CH=). IR cm⁻¹: 3290 (NH), 1625 (C=C). MS: *m/z* 325 [M+1]⁺. Anal. (C₁₇H₁₉N₅S) C, H, N, S.

General Procedure for the Synthesis of **5b,c.** 3-Chloroperoxybenzoic acid (2 mmol, 0.5 g of 77% suspension in mineral oil) was added portion wise to a solution of the opportune 6-(methylthio)-1-(2-phenylvinyl)-1*H*-pyrazolo[3,4-*d*]pyrimidin-4-amine (**4b** or **4c**) (1 mmol) in CHCl₃ (10 mL) at 0 °C. The mixture was stirred at room temperature for 6 h; the organic phase was washed with saturated NaHCO₃ solution (2 × 20 mL), then with water (20 mL), dried (MgSO₄), and evaporated under reduced pressure. The crude oil crystallized by adding a mixture of diethyl ether/petroleum ether (bp 40–60 °C) (1:1).

6-(Methylsulfonyl)-1-(2-phenylvinyl)-*N*-propyl-1*H*-pyrazolo[3,4-*d*]pyrimidin-4-amine (5b**).** White solid (0.20 g, 55%). Mp: 160–161 °C. ¹H NMR: δ 1.10 (t, *J* = 7.8, 3H, CH₃), 1.73 (sx, *J* = 7.8, 2H, CH₂CH₃), 3.41 (s, 3H, SO₂CH₃), 3.68 (q, *J* = 7.8, 2H, CH₂NH), 5.96 (br s, 1H, NH disappears with D₂O), 7.25–7.59 (m, 6H, 5Ar + CH=), 8.01 (d, *J*_{trans} = 14.4, 1H, CH=), 8.16 (s, 1H, H-3). IR cm⁻¹: 3341 (NH), 1618 (C=C), 1299, 1129 (SO₂). MS: *m/z* 357 [M+1]⁺. Anal. (C₁₇H₁₉N₅O₂S) C, H, N, S.

6-(Methylsulfonyl)-*N*-(2-phenylethyl)-1-(2-phenylvinyl)-1*H*-pyrazolo[3,4-*d*]pyrimidin-4-amine (5c**).** White solid (0.24 g, 57%). Mp: 138–139 °C (dec.). ¹H NMR: δ 3.05 (t, *J* = 6.0, 2H, CH₂Ar), 3.40 (s, 3H, SO₂CH₃), 3.98 (q, *J* = 6.0, 2H, CH₂NH), 6.18 (br s, 1H, NH disappears with D₂O), 7.18–7.57 (m, 11H, 10Ar + CH=), 8.02 (d, *J*_{trans} = 14.4, 1H, CH=), 8.13 (s, 1H, H-3). IR cm⁻¹: 3348 (NH), 1713 (C=C), 1298, 1127 (SO₂). MS: *m/z* 420 [M+1]⁺. Anal. (C₂₂H₂₁N₅O₂S) C, H, N, S.

Synthesis of 2-({4-[(2-Phenylethyl)amino]-1-(2-phenylvinyl)-1*H*-pyrazolo[3,4-*d*]pyrimidin-6-yl}-amino)ethanol (6c**).** 2-Aminoethanol (0.18 g, 3 mmol) was added to a suspension of **5c** (0.42 g, 1 mmol) in butan-1-ol (16 mL) and DMSO (4 mL), and the mixture was heated at 90 °C for 12 h. After cooling, butan-1-ol was removed under reduced pressure; then water was added, and the solution was extracted with ethyl acetate (2 × 20 mL); the organic phase was washed with water (20 mL), dried (MgSO₄), and evaporated under reduced pressure. The white solid was filtered and recrystallized from absolute ethanol (0.26 g, 65%). Mp: 83–84 °C. ¹H NMR: δ 2.99 (t, *J* = 7.0, 2H, CH₂Ar), 3.62–3.96 (m, 6H, CH₂NH + CH₂NH + CH₂OH), 5.40 (br s, 1H, disappears with D₂O), 5.61 (br s, 1H, disappears with D₂O), 7.18–7.44 (m, 11H, 10H Ar + CH=), 7.75 (s, 1H, H-3), 7.82 (d, *J*_{trans} = 14.4, 1H, CH=). IR cm⁻¹: 3250–3150 (OH + NH), 1656 (C=C). MS: *m/z* 401 [M+1]⁺. Anal. (C₂₃H₂₄N₆O) C, H, N.

Synthesis of 1-(2-Hydroxy-2-phenylethyl)-6-(methylsulfonyl)-1,5-dihydro-4*H*-pyrazolo[3,4-*d*]pyrimidin-4-one (8**).** 3-Chloroperoxybenzoic acid (20 mmol, 5 g of 77% suspension in mineral oil) was added portion wise to a solution of 1-(2-hydroxy-2-phenylethyl)-6-(methylthio)-1,5-dihydro-4*H*-pyrazolo[3,4-*d*]pyrimidin-4-one **7** (3.02 g, 10 mmol) in anhydrous DMF (5 mL) and CHCl₃ (50 mL) at 0 °C. The mixture was stirred at room temperature for 12 h. The solvent was evaporated under reduced pressure, and diethyl ether (20 mL) was added. By standing in a refrigerator for 2 h, a white solid was precipitated, which was filtered and recrystallized from absolute ethanol (1.91 g, 57%). Mp: 170–171 °C. ¹H NMR: δ 3.69 (s, 3H, SO₂CH₃), 4.22–4.52 (m, 2H, CH₂N), 4.91–5.09 (m, 1H, CHO), 5.60 (br s, 1H, OH disappears with D₂O), 7.09–7.28 (m, 5H Ar), 8.15 (s, 1H, H-3), 13.20 (br s, 1H, NH disappears with D₂O). IR cm⁻¹: 3540 (NH), 3150–2900 (OH), 1693 (CO). MS: *m/z* 334 [M+1]⁺. Anal. (C₁₄H₁₄N₄O₄S) C, H, N, S.

Synthesis of 1-(2-Hydroxy-2-phenylethyl)-6-morpholin-4-yl-1,5-dihydro-4*H*-pyrazolo[3,4-*d*]pyrimidin-4-one (9**).** Morpholine (4.36 g, 50 mmol) was added to a solution of 1-(2-hydroxy-2-phenylethyl)-6-(methylsulfonyl)-1,5-dihydro-4*H*-pyrazolo[3,4-*d*]pyrimidin-4-one **8** (3.34 g, 10 mmol) in DMSO (30 mL), and the mixture was heated at 100 °C for 3 h. After cooling to room temperature, cold water was added;

the pale yellow solid was filtered, washed with water, and recrystallized from 95% ethanol (2.29 g, 67%). Mp: 247–248 °C. $^1\text{H NMR}$: δ 3.36–3.49 and 3.51–3.62 (2 m, 8H, 4CH_2 morph.), 3.99–4.25 (m, 2H, CH_2N), 4.90–5.03 (m, 1H, CHO), 5.50 (d, 1H, OH disappears with D_2O), 7.03–7.24 (m, 5H Ar), 7.70 (s, 1H, H-3), 10.75 (br s, 1H, NH disappears with D_2O). IR cm^{-1} : 3380, 3168, 3113 (NH + OH), 1702 (CO). MS: m/z 341 $[\text{M}+1]^+$. Anal. ($\text{C}_{17}\text{H}_{19}\text{N}_5\text{O}_3$) C, H, N.

Synthesis of 4-Chloro-1-(2-chloro-2-phenylethyl)-6-morpholin-4-yl-1H-pyrazolo[3,4-d]pyrimidine (10). The Vilsmeier complex, previously prepared from POCl_3 (3.07 g, 20 mmol) and anhydrous DMF (1.46 g, 20 mmol), was added to a suspension of 1-(2-hydroxy-2-phenylethyl)-6-morpholin-4-yl-1,5-dihydro-4H-pyrazolo[3,4-d]pyrimidin-4-one **9** (0.34 g, 1 mmol) in CHCl_3 (10 mL). The mixture was refluxed for 12 h. The solution was washed with 4 M NaOH (2 \times 20 mL), then with water (20 mL), dried (MgSO_4), and concentrated under reduced pressure. The crude was purified by column chromatography (Florisil, 100–200 mesh) using diethyl ether as the eluant, to afford the pure product as a yellow oil, which was crystallized as a white solid by adding a mixture of diethyl ether/petroleum ether (bp 40–60 °C) (1:1) and standing in a refrigerator (0.25 g, 67%). Mp: 117–118 °C. $^1\text{H NMR}$: δ 3.47–3.56 and 3.60–3.68 (2 m, 8H, 4CH_2 morph.), 4.53–4.70 (m, 2H, CH_2N), 5.40–5.50 (m, 1H, CHCl), 7.15–7.38 (m, 5H Ar), 7.73 (s, 1H, H-3). MS: m/z 378 $[\text{M}+1]^+$. Anal. ($\text{C}_{17}\text{H}_{17}\text{N}_5\text{Cl}_2\text{O}$) C, H, N.

Synthesis of *N*-(3-Chlorophenyl)-1-(2-chloro-2-phenylethyl)-6-morpholin-4-yl-1H-pyrazolo[3,4-d]pyrimidin-4-amine (11). A solution of 4-chloro-1-(2-chloro-2-phenylethyl)-6-morpholin-4-yl-1H-pyrazolo[3,4-d]pyrimidine **10** (0.38 g, 1 mmol) and 3-chloroaniline (0.50 g, 4 mmol) in absolute ethanol was refluxed for 5 h. After cooling, the solvent was evaporated under reduced pressure, and the crude was treated with water (20 mL), then extracted with CHCl_3 (20 mL); the organic phase was washed with water (20 mL), dried (MgSO_4), and concentrated under reduced pressure. The obtained oil was crystallized by adding a mixture of diethyl ether/petroleum ether (bp 40–60 °C) (1:1) and standing in a refrigerator to afford a white solid, which was recrystallized from absolute ethanol (0.27 g, 57%). Mp: 168–170 °C. $^1\text{H NMR}$: δ 3.45–3.54 and 3.59–3.66 (2 m, 8H, 4CH_2 morph.), 4.51–4.68 (m, 2H, CH_2N), 5.41–5.55 (m, 1H, CHCl), 7.00–7.56 (m, 10H, 9 Ar + H-3). IR cm^{-1} : 3356 (NH). MS: m/z 469 $[\text{M}+1]^+$. Anal. ($\text{C}_{23}\text{H}_{22}\text{N}_6\text{Cl}_2\text{O}$) C, H, N.

Synthesis of 1-(2-Hydroxy-2-phenylethyl)-6-[(2-morpholin-4-ylethyl)thio]-1,5-dihydro-4H-pyrazolo[3,4-d]pyrimidin-4-one (13). NaOH (0.4 g, 10 mmol) dissolved in absolute ethanol (5 mL) and 4-(2-chloroethyl)morpholine (2.24 g, 15 mmol) were added to a solution of 1-(2-hydroxy-2-phenylethyl)-6-thio-1,5,6,7-tetrahydro-4H-pyrazolo[3,4-d]pyrimidin-4-one **12** (2.88 g, 10 mmol) in anhydrous DMF (5 mL). The solution was refluxed for 6 h. After cooling, the solvent was evaporated under reduced pressure, and the crude was poured into cold water. The white solid was filtered, washed with water, and recrystallized from absolute ethanol (2.53 g, 63%). Mp: 201–202 °C. $^1\text{H NMR}$: δ 2.36–2.50 (m, 4H, $2\text{CH}_2\text{N}$ morph.), 3.10–3.40 (m, 4H, CH_2S + $\text{CH}_2\text{CH}_2\text{S}$), 3.45–3.56 (m, 4H, $2\text{CH}_2\text{O}$ morph.), 4.13–4.40 (m, 2H, CH_2N), 4.83–5.06 (m, 1H, CHO), 5.55 (d, 1H, OH disappears with D_2O), 7.10–7.28 (m, 5H Ar), 7.89 (s, 1H, H-3). IR cm^{-1} : 3100–2850 (NH + OH), 1664 (CO). MS: m/z 401 $[\text{M}+1]^+$. Anal. ($\text{C}_{19}\text{H}_{23}\text{N}_5\text{O}_3\text{S}$) C, H, N, S.

Synthesis of 4-Chloro-1-(2-chloro-2-phenylethyl)-6-[(2-morpholin-4-ylethyl)thio]-1H-pyrazolo[3,4-d]pyrimidine (14). The Vilsmeier complex, previously prepared from POCl_3 (12.27 g, 80 mmol) and anhydrous DMF (5.85 g, 80 mmol) was added to a suspension of 1-(2-hydroxy-2-phenylethyl)-6-[(2-morpholin-4-ylethyl)thio]-1,5-dihydro-4H-pyrazolo[3,4-d]pyrimidin-4-one **13** (4.01 g, 10 mmol) in CHCl_3 (50 mL). The mixture was refluxed for 8 h. The solution was washed with 4 M NaOH (2 \times 20 mL), then with water (20 mL), dried (MgSO_4), and concentrated under reduced pressure.

The yellow crude oil was crystallized as a brown solid by adding absolute ethanol and standing in a refrigerator (3.29 g, 75%). Mp: 106–107 °C. $^1\text{H NMR}$: δ 2.81–3.12 (m, 4H, $2\text{CH}_2\text{N}$ morph.), 3.18–3.81 (m, 4H, CH_2S + $\text{CH}_2\text{CH}_2\text{S}$), 3.86–4.10 (m, 4H, $2\text{CH}_2\text{O}$ morph.), 4.60–4.78 and 5.12–5.30 (2 m, 2H, CH_2N), 5.36–5.50 (m, 1H, CHCl), 7.16–7.50 (m, 5H Ar), 8.00 (s, 1H, H-3). MS: m/z 438 $[\text{M}+1]^+$. Anal. ($\text{C}_{19}\text{H}_{21}\text{N}_5\text{Cl}_2\text{OS}$) C, H, N, S.

General Procedure for the Synthesis of Compounds 15a–d. The appropriate amine (40 mmol) was added to a solution of the 4-chloro derivative **14** (4.38 g, 10 mmol) in anhydrous toluene (10 mL), and the mixture was stirred at room temperature for 24 h. The organic phase was washed with water (2 \times 10 mL), dried (MgSO_4), and concentrated under reduced pressure. The crude oil was crystallized by adding diethyl ether.

General Procedure for the Synthesis of Compounds 15e,f. The appropriate aniline (20 mmol) was added to a solution of the 4-chloro derivative **14** (4.38 g, 10 mmol) in absolute ethanol (5 mL), and the mixture was refluxed for 3–5 h. After cooling to room temperature, the solid was filtered, washed with water, and recrystallized from absolute ethanol.

1-(2-Chloro-2-phenylethyl)-6-[(2-morpholin-4-ylethyl)thio]-*N*-propyl-1H-pyrazolo[3,4-d]pyrimidin-4-amine (15a). White solid (2.77 g, 60%). Mp: 86–87 °C. $^1\text{H NMR}$: δ 0.95 (t, $J = 7.2$, 3H, CH_3), 1.63 (sx, $J = 7.2$, 2H, CH_2CH_3), 2.52 (t, $J = 4.6$, 4H, $2\text{CH}_2\text{N}$ morph.), 2.62–2.78 (m, 2H, $\text{CH}_2\text{CH}_2\text{S}$), 3.10–3.33 (m, 2H, CH_2S), 3.46 (q, $J = 7.2$, 2H, CH_2NH), 3.67 (t, $J = 4.6$, 4H, $2\text{CH}_2\text{O}$ morph.), 4.53–4.67 and 4.74–4.80 (2 m, 2H, CH_2N), 5.30 (br s, 1H, NH disappears with D_2O), 5.38–5.51 (m, 1H, CHCl), 7.12–7.42 (m, 5H Ar), 7.71 (s, 1H, H-3). IR cm^{-1} : 3281 (NH). MS: m/z 461 $[\text{M}+1]^+$. Anal. ($\text{C}_{22}\text{H}_{29}\text{N}_6\text{OClS}$) C, H, N, S.

***N*-Benzyl-1-(2-chloro-2-phenylethyl)-6-[(2-morpholin-4-ylethyl)thio]-1H-pyrazolo[3,4-d]pyrimidin-4-amine (15b).** White solid (3.56 g, 70%). Mp: 124–125 °C. $^1\text{H NMR}$: δ 2.50 (t, $J = 4.4$, 4H, $2\text{CH}_2\text{N}$ morph.), 2.64–2.81 (m, 2H, $\text{CH}_2\text{CH}_2\text{S}$), 3.10–3.38 (m, 2H, CH_2S), 3.58–3.72 (m, 4H, $2\text{CH}_2\text{O}$ morph.), 4.53–4.94 (m, 4H, CH_2N + CH_2Ar), 5.40–5.52 (m, 1H, CHCl), 7.12–7.42 (m, 10H Ar), 7.66 (s, 1H, H-3). IR cm^{-1} : 3197 (NH). MS: m/z 509 $[\text{M}+1]^+$. Anal. ($\text{C}_{26}\text{H}_{29}\text{N}_6\text{OClS}$) C, H, N, S.

1-(2-Chloro-2-phenylethyl)-*N*-(4-fluorobenzyl)-6-[(2-morpholin-4-ylethyl)thio]-1H-pyrazolo[3,4-d]pyrimidin-4-amine (15c). White solid (3.16 g, 60%). Mp: 86–87 °C. $^1\text{H NMR}$: δ 2.55 (t, $J = 4.6$, 4H, $2\text{CH}_2\text{N}$ morph.), 2.70–2.83 (m, 2H, $\text{CH}_2\text{CH}_2\text{S}$), 3.00–3.29 (m, 2H, CH_2S), 3.55–3.68 (m, 4H, $2\text{CH}_2\text{O}$ morph.), 4.55–5.00 (m, 4H, CH_2N + CH_2Ar), 5.43–5.54 (m, 1H, CHCl), 7.07–7.39 (m, 9H Ar), 7.67 (s, 1H, H-3). IR cm^{-1} : 3280 (NH). MS: m/z 527 $[\text{M}+1]^+$. Anal. ($\text{C}_{26}\text{H}_{28}\text{N}_6\text{OClFS}$) C, H, N, S.

1-(2-Chloro-2-phenylethyl)-6-[(2-morpholin-4-ylethyl)thio]-*N*-(2-phenylethyl)-1H-pyrazolo[3,4-d]pyrimidin-4-amine (15d). White solid (3.40 g, 65%). Mp: 122–123 °C. $^1\text{H NMR}$: δ 2.51 (t, $J = 4.6$, 4H, $2\text{CH}_2\text{N}$ morph.), 2.72 (t, $J = 7.6$, 2H, $\text{CH}_2\text{CH}_2\text{S}$), 2.91 (t, $J = 6.4$, 2H, CH_2Ar), 3.10–3.36 (m, 2H, CH_2S), 3.66 (t, $J = 4.6$, 4H, $2\text{CH}_2\text{O}$ morph.), 3.79 (q, $J = 6.4$, 2H, CH_2NH), 4.54–4.70 and 4.75–4.90 (2 m, 2H, CH_2N), 5.30 (br s, 1H, NH disappears with D_2O), 5.40–5.52 (m, 1H, CHCl), 7.10–7.41 (m, 10H Ar), 7.63 (s, 1H, H-3). IR cm^{-1} : 3251 (NH). MS: m/z 523 $[\text{M}+1]^+$. Anal. ($\text{C}_{27}\text{H}_{31}\text{N}_6\text{OClS}$) C, H, N, S.

***N*-(3-Chlorophenyl)-1-(2-chloro-2-phenylethyl)-6-[(2-morpholin-4-ylethyl)thio]-1H-pyrazolo[3,4-d]pyrimidin-4-amine (15e).** White solid (3.70 g, 70%). Mp: 223–224 °C. $^1\text{H NMR}$: δ 2.88–4.00 (m, 12H, 4CH_2 morph. + $\text{CH}_2\text{CH}_2\text{S}$ + CH_2S), 4.65–4.83 and 5.00–5.18 (2 m, 2H, CH_2N), 5.53–5.68 (m, 1H, CHCl), 7.00–8.40 (m, 10H, 9Ar + H-3), 11.50 (br s, 1H, NH disappears with D_2O). IR cm^{-1} : 3262 (NH). MS: m/z 529 $[\text{M}+1]^+$. Anal. ($\text{C}_{25}\text{H}_{26}\text{N}_6\text{OCl}_2\text{S}$) C, H, N, S.

1-(2-Chloro-2-phenylethyl)-6-[(2-morpholin-4-ylethyl)thio]-*N*-phenyl-1H-pyrazolo[3,4-d]pyrimidin-4-amine (15f). White solid (3.37 g, 68%). Mp: 227–228 °C. $^1\text{H NMR}$: δ 2.85–4.00 (m, 12H, 4CH_2

morph. + $\text{CH}_2\text{CH}_2\text{S} + \text{CH}_2\text{S}$), 4.70–4.85 and 4.96–5.20 (2 m, 2H, CH_2N), 5.60–5.70 (m, 1H, CHCl), 6.80–8.30 (m, 11H, 10Ar + H-3), 12.00 (br s, 1H, NH disappears with D_2O). IR cm^{-1} : 3270 (NH). MS: m/z 495 $[\text{M}+1]^+$. Anal. ($\text{C}_{25}\text{H}_{27}\text{N}_6\text{ClOS}$) C, H, N, S.

General Procedure for the Synthesis of Compounds 17a–d. To a solution of the opportune intermediate **16a,b** (1.5 equiv) in dioxane (2 mL), the opportune amine (1.5 equiv) and glacial acetic acid (1.5 equiv) were added. The reaction mixture was irradiated in the microwave for 10 min at 150 °C. After cooling, the mixture was evaporated under reduced pressure, and the crude purified by flash chromatography using a mixture of $\text{CH}_2\text{Cl}_2/\text{MeOH}$ (97:3) as the eluent to give the pure products as yellow solids.

1-[2-Chloro-2-(4-fluorophenyl)ethyl]-N-(pyridin-4-ylmethyl)-1H-pyrazolo[3,4-d]pyrimidin-4-amine (**17a**). Yellow solid (42 mg, 58%). Mp: 144–145 °C. ^1H NMR: δ 4.75–5.00 (m, 4H, $\text{CH}_2\text{N} + \text{CH}_2\text{Ar}$), 5.50–5.55 (m, 1H, CHCl), 7.19–7.33 (m, 6H, Ar), 7.90 (s, 1H, H-3), 8.39 (s, 1H, H-6), 8.48 (m, 2H, Ar). MS: m/z 383 $[\text{M}+1]^+$. Anal. ($\text{C}_{19}\text{H}_{16}\text{N}_6\text{ClF}$) C, H, N.

1-[2-Chloro-2-(4-fluorophenyl)ethyl]-N-(pyridin-2-ylmethyl)-1H-pyrazolo[3,4-d]pyrimidin-4-amine (**17b**). Yellow solid (42 mg, 58%). Mp: 137–138 °C. ^1H NMR: δ 4.76–4.98 (m, 4H, $\text{CH}_2\text{N} + \text{CH}_2\text{Ar}$), 5.51–5.57 (m, 1H, CHCl), 6.81–7.72 (m, 7H, Ar), 7.99 (s, 1H, H-3), 8.41 (s, 1H, H-6), 8.61 (m, 1H, Ar). MS: m/z 383 $[\text{M}+1]^+$. Anal. ($\text{C}_{19}\text{H}_{16}\text{N}_6\text{ClF}$) C, H, N.

1-[2-Chloro-2-(4-chlorophenyl)ethyl]-N-(pyridin-4-ylmethyl)-1H-pyrazolo[3,4-d]pyrimidin-4-amine (**17c**). Yellow solid (51 mg, 70%). Mp: 144–145 °C. ^1H NMR: δ 4.68–4.90 (m, 4H, $\text{CH}_2\text{N} + \text{CH}_2\text{Ar}$), 5.40–5.46 (m, 1H, CHCl), 7.23–7.32 (m, 6H, Ar), 7.78 (s, 1H, H-3), 8.32 (s, 1H, H-6), 8.48 (m, 2H, Ar). MS: m/z 399 $[\text{M}+1]^+$. Anal. ($\text{C}_{19}\text{H}_{16}\text{N}_6\text{Cl}_2$) C, H, N.

1-[2-Chloro-2-(4-chlorophenyl)ethyl]-N-(pyridin-2-ylmethyl)-1H-pyrazolo[3,4-d]pyrimidin-4-amine (**17d**). Yellow solid (46 mg, 63%). Mp: 137–138 °C. ^1H NMR: δ 4.75–4.91 (m, 4H, $\text{CH}_2\text{N} + \text{CH}_2\text{Ar}$), 5.50–5.55 (m, 1H, CHCl), 7.24–7.31 (m, 4H, Ar), 7.37 (d, J = 8, 4H, Ar), 7.71 (t, J = 8.0, 1H, Ar), 7.98 (s, 1H, H-3), 8.41 (s, 1H, H-6), 8.61 (m, 1H, Ar). MS: m/z 399 $[\text{M}+1]^+$. Anal. ($\text{C}_{19}\text{H}_{16}\text{N}_6\text{Cl}_2$) C, H, N.

Enzymatic Assays. *Enzymatic Assay on Isolated Src.* Recombinant human Src was purchased from Upstate (Lake Placid, NY). Activity was measured in a filter-binding assay using a commercial kit (Src Assay Kit, Upstate), according to the manufacturer's protocol, using 150 μM of the specific Src peptide substrate (KVEKIGEGTYGVVYK) and in the presence of 0.125 pmol of Src and 0.160 pmol of $[\gamma\text{-}^{32}\text{P}]\text{-ATP}$. The apparent affinity (K_m) values of the Src preparation used for its peptide and ATP substrates were determined separately and found to be 30 μM and 5 μM , respectively.

Kinetic Analysis. Dose–response curves were generated by fitting the data by computer simulation to eq 1: $E_{(\%)}$ = $E_{\text{max}}/(1 + [\text{I}]/\text{ID}_{50})$, where $E_{(\%)}$ is the fraction of the enzyme activity measured in the presence of the inhibitor, E_{max} is the activity in the absence of the inhibitor, $[\text{I}]$ is the inhibitor concentration, and ID_{50} is the inhibitor concentration at which $E_{(\%)} = 0.5E_{\text{max}}$. The ID_{50} values were converted to K_i according to a competitive mechanism with respect to the substrate ATP. The second substrate of the reaction (the peptide) was kept at saturating concentrations (4-fold higher its K_m). Since (i) the ATP concentration was limiting, i.e., $[\text{ATP}] \ll K_m(\text{ATP})$, and (ii) the enzyme concentration was not negligible with respect to the ATP concentration, i.e., $[\text{E}] \geq [\text{ATP}]$, the classical Cheng-Prusoff relationship was not applicable. Consequently, K_i values were calculated according to eq 2: $K_i = (\text{ID}_{50} - E_0/2)/\{E_0 - [S_0/K_m - 1]/E_0\}$, where S_0 is the concentration of the competing substrate (ATP), and E_0 is the concentration of the enzyme. Each experiment was done in triplicate, and mean values were used for the interpolation. Curve fitting was performed with the program GraphPad Prism.

Enzymatic Assay on Isolated Abl. Recombinant human Abl was purchased from Upstate. Activity was measured in a filter-binding assay

using an Abl specific peptide substrate (Abtide, Upstate). Reaction conditions were as follows: 0.012 μM $[\gamma\text{-}^{32}\text{P}]\text{ATP}$, 50 μM peptide, and 0.022 μM c-Abl. The apparent affinity (K_m) values of the Abl preparation used for its peptide and ATP substrates were determined separately and found to be 1.5 μM and 10 μM , respectively. Kinetic analysis was performed as described for c-Src. Because of the noncompetitive mode of action and because of the fact that the enzyme concentration was higher than the ATP substrate concentration, ID_{50} values were converted to K_i by eq 3: $K_i = \text{ID}_{50}/\{E_0 + [E_0(K_m(\text{ATP})/S_0)]\}/E_0$, where E_0 and S_0 are the enzyme and the ATP concentrations, respectively. Each experiment was done in triplicate, and mean values were used for the interpolation. Curve fitting was performed with the program GraphPad Prism.

ADME Assays. *Chemicals and Instruments.* All solvents, reagents, and L- α -phosphatidylcholine were from Sigma-Aldrich Srl (Milan, Italy). Dodecane was purchased from Fluka (Milan, Italy). Pooled Male Donors 20 mg/mL HLM were from BD Gentest-Biosciences (San Jose, California). Milli-Q quality water (Millipore, Milford, MA, USA) was used. Hydrophobic filter plates (MultiScreen-IP, Clear Plates, 0.45 μm -diameter pore size), 96-well microplates, and 96-well UV-transparent microplates were obtained from Millipore (Bedford, MA, USA).

LC analyses for the PAMPA studies were performed with a Perkin-Elmer HPLC (series 200) equipped with an injector valve, a 20- μL sample loop (Mod. Rheodyne), and a UV detector (Perkin-Elmer 785A, UV/vis Detector). UV detection was monitored at 254 nm.

LC analyses for the solubility and metabolic stability studies were performed with an Agilent 1100 LC/MSD VL system (G1946C) (Agilent Technologies, Palo Alto, CA) constituted by a vacuum solvent degassing unit, a binary high-pressure gradient pump, an 1100 series UV detector, and an 1100 MSD model VL benchtop mass spectrometer. The Agilent 1100 series mass spectra detection (MSD) single-quadrupole instrument was equipped with the orthogonal spray API-ES (Agilent Technologies, Palo Alto, CA). Nitrogen was used as nebulizing and drying gas. The pressure of the nebulizing gas, the flow of the drying gas, the capillary voltage, the fragmentor voltage, and the vaporization temperature were set at 40 psi, 9 L/min, 3000 V, 70 V, and 350 °C, respectively. UV detection was monitored at 254 nm. The LC-ESI-MS determination was performed by operating the MSD in the positive ion mode. Spectra were acquired over the scan range m/z 100–1500 using a step size of 0.1 us.

Parallel Artificial Membrane Permeability Assay (PAMPA). Donor solution (0.5 mM) was prepared by diluting 1 mM dimethyl sulfoxide (DMSO) compound stock solution using phosphate buffer (pH 7.4, 0.025 M). Filters were coated with 5 μL of a 1% (w/v) dodecane solution of phosphatidylcholine. Donor solution (150 μL) was added to each well of the filter plate. To each well of the acceptor plate were added 300 μL of solution (50% DMSO in phosphate buffer). All compounds were tested in three different plates on different days. The sandwich was incubated for 5 h at room temperature under gentle shaking. After the incubation time, the sandwich plates were separated, and samples were taken from both receiver and donor sides and analyzed using LC with UV detection. LC analyses were conducted via HPLC (Perkin-Elmer series 200) using a Polaris C_{18} column (150 \times 4.6 mm, 5 μm particle size) at a flow rate of 0.8 $\text{mL} \cdot \text{min}^{-1}$ with a mobile phase composed of 80% ACN/20% H_2O –formic acid 0.1% (for compounds **1**, **5c**, **11**, **19**, and **20**) or 60% ACN/40% H_2O –formic acid 0.1% (for compounds **17c**, **15b**, **15e**, and **15f**). Permeability (P_{app}) for PAMPA was calculated according to the following equation obtained from Wohnsland and Faller⁴³ and Sugano et al.⁴⁴ with some modification in order to obtain permeability values in cm^2/s :

$$P_{\text{app}} = \frac{V_D V_A}{(V_D + V_A) A t} - \ln(1 - r)$$

where V_A is the volume in the acceptor well, V_D is the volume in the donor well (cm^3), A is the “effective area” of the membrane (cm^2),

t is the incubation time (s), and r is the ratio between drug concentration in the acceptor and equilibrium concentration of the drug in the total volume ($V_D + V_A$). Drug concentration is estimated by using the peak area integration.

Solubility Assay. Stock solutions of each compound in 10^{-3} M DMSO were prepared and sequentially diluted to reach the 10^{-6} M concentration. Four different aliquots (1.0, 1.5, 3.0, and 6.0 μL) of each 10^{-6} M stock solution of all compounds were dispensed into well plates with the necessary amount of water to reach the final volume of 300 μL . Wells were shaken in a shaker bath at room temperature for 24 h.³⁶ These suspensions were filtered through a 0.45- μm nylon filter (Acrodisc), proceeding with the chromatographic assays, performed in triplicate for each compound. Quantitative analysis was performed by means of the LC-UV method above-reported. LC analyses were conducted via HPLC (Agilent 1100 LC/MSD VL system) using a Varian Polaris 5 C18-A column (150 \times 4.6 mm, 5 μm particle size) maintained at room temperature at a flow rate of 0.8 mL \cdot min⁻¹ with a mobile phase composed of 70% ACN/30% H₂O (for compounds **1**, **5c**, **11**, **15b**, **15e**, **15f**, **17c**, and **20**) or 80% ACN/20% H₂O–formic acid 0.1% (for compound **19**).

Microsomal Stability Assay. Each compound in DMSO solution was incubated at 37 °C for 60 min in 125 mM phosphate buffer (pH 7.4), 5 μL of human liver microsomal protein (0.2 mg/mL), in the presence of a NADPH-generating system at a final volume of 0.5 mL (compounds' final concentration, 100 μM); DMSO did not exceed 2% (final solution).⁴⁵ The reaction was stopped by cooling in ice and adding 1.0 mL of acetonitrile. The reaction mixtures were then centrifuged, and the parent drug and metabolites were subsequently determined by LC-MS.

Quantitative and qualitative analysis was performed by means of the LC-UV method above-reported. LC analyses were conducted via HPLC (Agilent 1100 LC/MSD VL system) using a Varian Polaris 5 C18-A column (150 \times 4.6 mm, 5 μm particle size) maintained at room temperature. Chromatographic analysis was carried out using gradient elution with eluent A being ACN and eluent B consisting of an aqueous solution of formic acid (0.1%). The analysis started with 10% of eluent A, which was rapidly increased up to 70% in 10 min, then slowly increased up to 98% in 15 min, and finally returned to 10% of eluent A in 1.0 min. The flow rate was 0.8 mL min⁻¹, and injection volume was 5 μL .

Cell assay. Human CML K-562 cell lines in blast crisis⁴⁶ were obtained from the American Type Culture Collection and were grown in RPMI 1640 medium (Euroclone, Devon, UK), containing 10% fetal bovine serum (FBS) and antibiotics (100 U/mL penicillin and 100 μg /mL streptomycin). The cultures were free of mycoplasma. Cells were cultured in normoxic or hypoxic conditions. For the experiments in normoxia, we used an incubator (KW Apparacchi Scientifici, Italy) set at 5% CO₂, 20% O₂ (atmospheric oxygen \approx 140 mmHg), and 37 °C in a humidified environment. For the experiments under hypoxia, we used a water-jacketed incubator (Forma Scientific, Marietta, OH), which provides a customized and stable humidified environment through electronic control of CO₂ (5%), O₂, and temperature (37 °C). In our experiments, the O₂ tension was set and maintained constantly at 2% (\approx 14 mmHg) by injecting N₂ automatically in the chamber to bring the O₂ level to the set point.⁴⁷ The compounds were dissolved in DMSO and used at the indicated concentrations. At the end of the experiments, cells were promptly analyzed.

CyQUANT Cell Proliferation Assay. To quantify cell proliferation, starved cells were plated into 96 well plates in RPMI containing FBS at the concentration of 1×10^4 cells/well and then incubated for 72 h, with or without different concentrations (0.5–150 μM) of the studied compounds, in normoxic or hypoxic conditions. At the end, each culture microplate was centrifuged, reversed to remove growth medium, and kept at -80 °C. The microplates were then thawed at room temperature, and 200 μL of the CyQUANT GR dye/cell-lysis buffer (Molecular Probes, Eugene, OR) was added to each sample well. The concentrated cell-lysis buffer was diluted 1:20 into ultrapure water, and CyQUANT

GR dye was then diluted 1:400 into lysis buffer. The samples were incubated in darkness for 2 to 5 min prior to measuring relative fluorescence (485 nm excitation, 520 nm emission) using a fluorescence microplate reader FLUOstar OPTIMA (BMG Labtech, Offenburg, Germany). Data analysis for IC₅₀ calculations was performed with the LSW Data Analysis Package plug-in for Excel (Microsoft). Results are reported as the mean \pm SEM.

Western Blot Analysis. The inhibitory effect of compounds toward the phosphorylation of Src (Tyr416), c-Abl, and STAT-5 was assessed using immunoblot analysis, as previously described.⁴⁸ Cell lines were cultured at a concentration of 1×10^6 cells/mL and challenged with the compounds (50 μM) for 3 h in normoxic or hypoxic conditions. Later, cells were harvested and lysed in an appropriate buffer containing 1% Triton X-100. Proteins were quantitated by the BCA method (Pierce, Rockford, IL). Equal amounts of total cellular protein were resolved by SDS-PAGE under nonreducing conditions, transferred to a PVDF membrane, and subjected to immunoblot using phospho-specific antibodies against Src (Cell Signaling Technology, Beverly, MA) and a PathScan Bcr/Abl Activity Assay Western Detection Kit (Cell Signaling Technology) for c-Abl and STAT-5. This kit was used to assay the inhibition of multiple proteins on one membrane without stripping and reprobing. Filters were additionally probed with β -actin (control loading, Cell Signaling Technology).

The proapoptotic activity of the selected compounds was also tested, using immunoblot analysis with a PARP-specific antibody that reveals both the uncleaved (113 kDa) and cleaved (89 kDa) forms of PARP (Cell Signaling Technology). Cell lines were cultured at a concentration of 1.4×10^6 cells/mL and challenged with the compounds (10 μM) for 72 h in normoxic or hypoxic conditions.

Caspase assay. Intracellular caspase-3 activity was measured using an EnzCheck Caspase-3 Assay kit (Molecular Probes), as previously described.⁴⁸ Briefly, cells (2×10^6 cells/mL) were exposed to either 21% O₂ or 2% O₂ for 72 h in the presence or in the absence of selected compounds (10 μM), harvested, and washed with PBS. Cells were then lysed and added with the specific caspase-3 fluorogenic substrate. Fluorescence was then quantified by the microplate reader FLUOstar Optima with excitation at 496 nm and emission at 520 nm.

RNA Preparation and qRT-PCR. CA IX mRNA expression was determined by qRT-PCR using an iQ5Multicolor Real-Time PCR Detection System (Bio-Rad Laboratories). Briefly, tumor cells (7×10^5 cells/mL) were exposed to either 21% O₂ or 2% O₂ for 72 h in the presence or in the absence of selected compounds (10 μM), and total RNA was extracted using the TRI Reagent (Ambion, Austin, TX). First-strand cDNA synthesis was performed using the iScript cDNA Synthesis Kit (Bio-Rad Laboratories). qRT-PCR was performed using iTaq SYBR Green Supermix with ROX (Bio-Rad Laboratories), and the specific primers were designed using the PRIMER3 program (available at <http://frodo.wi.mit.edu>). Data were quantitatively analyzed on iQ5 Optical System Software (Bio-Rad Laboratories). Relative quantification was done by using the $2^{-\Delta\Delta\text{CT}}$ method, as previously described;⁴⁹ β -actin was used as a housekeeping gene, and results were reported as mRNA expression versus the control cells.

■ ASSOCIATED CONTENT

Supporting Information. Details on the synthesis data of compound **19**, a table with elemental analysis for the new synthesized compounds, and a table with predicted metabolites. This material is available free of charge via the Internet at <http://pubs.acs.org>.

■ AUTHOR INFORMATION

Corresponding Author

*(S.S.) Dipartimento di Scienze Farmaceutiche, Università degli Studi di Genova, Viale Benedetto XV 3, 16132 Genova, Italy.

Phone: +39 010 3538866. Fax: +39 010 3538358. E-mail: schensil@unige.it. (M.B.) Dipartimento Farmaco Chimico Tecnologico, Università degli Studi di Siena, Via Alcide de Gasperi 2, I-53100 Siena, Italy. Phone: +39 0577 234306. Fax: +39 0577 234306. E-mail: botta.maurizio@gmail.com.

ACKNOWLEDGMENT

This work was partially supported by the Italian Association for Cancer Research AIRC IG 4538 grant to G.M. and by National Interest Research Projects (PRIN_2007_N7KYCY) to G.M., M.B., and S.S. (PRIN_2008_5HRSJK). Fondazione Monte dei Paschi di Siena is also acknowledged for financial support (Grant No. 35023/2008). E.C. was the recipient of an FIRC Fellowship. M.B. thanks Prof. Gabriele Cruciani (Molecular Discovery, Ltd.) for kindly providing the software Metasite.

ABBREVIATIONS USED

CML, chronic myeloid leukemia; Ph, Philadelphia; IM, imatinib; TKIs, tyrosine kinase inhibitors; WT, wild type; PK, pharmacokinetic; HIF-1, hypoxia-inducible factor-1; STAT-5, signal transducer and activator of transcription 5; PARP, poly-ADP-ribose-polymerase; CA, carbonic anhydrases; PAMPA, parallel artificial membrane permeability assay; HLM, human liver microsome; GA, genetic algorithm.

REFERENCES

- (1) Quintas Cardama, A.; Cortes, J. Molecular biology of bcr-abl1 positive chronic myeloid leukemia. *Blood* **2009**, *113*, 1619–1630.
- (2) Groffen, J.; Stephenson, J. R.; Heisterkamp, N.; de Klein, A.; Bartram, C. R.; Grosveld, G. Philadelphia chromosomal breakpoints are clustered within a limited region, bcr, on chromosome 22. *Cell* **1984**, *36*, 93–99.
- (3) Palandri, F.; Iacobucci, I.; Castagnetti, F.; Testoni, N.; Poerio, A.; Amabile, M.; Breccia, M.; Intermesoli, T.; Iuliano, F.; Rege-Cambrin, G.; Tiribelli, M.; Miglino, M.; Pane, F.; Saglio, G.; Martinelli, G.; Rosti, G.; Baccarani, M. Front-line treatment of Philadelphia positive chronic myeloid leukemia with imatinib and interferon-alpha: 5-year outcome. *Haematologica* **2008**, *93*, 770–774.
- (4) Apperley, J. F. Part I: mechanisms of resistance to imatinib in chronic myeloid leukaemia. *Lancet Oncol.* **2007**, *8*, 1018–1029.
- (5) Sawyers, C. Targeted cancer therapy. *Nature* **2004**, *432*, 294–297.
- (6) (a) Petrelli, A.; Giordano, S. From single- to multi-target drugs in cancer therapy: when aspecificity becomes an advantage. *Curr. Med. Chem.* **2008**, *15*, 422–432. (b) Knight, Z. A.; Lin, H.; Shokat, K. M. Targeting the cancer kinome through polypharmacology. *Nat. Rev. Cancer* **2010**, *10*, 130–137.
- (7) Hiles, J. J.; Kolesar, J. M. Role of sunitinib and sorafenib in the treatment of metastatic renal cell carcinoma. *Am. J. Health Syst. Pharm.* **2008**, *65*, 123–131.
- (8) Heinrich, M. C.; Griffith, D. J.; Druker, B. J.; Wait, C. L.; Ott, K. A.; Ziegler, A. J. Inhibition of c-kit receptor tyrosine kinase activity by STI 571, a selective tyrosine kinase inhibitor. *Blood* **2000**, *96*, 925–932.
- (9) (a) Radi, M.; Schenone, S.; Botta, M. Allosteric inhibitors of Bcr-Abl: towards novel myristate-pocket binders. *Curr. Pharm. Biotechnol.* **2011** in press. (b) Zhang, J.; Adrián, F. J.; Jahnke, W.; Cowan-Jacob, S. W.; Li, A. G.; Iacob, R. E.; Sim, T.; Powers, J.; Dierks, C.; Sun, F.; Guo, G. R.; Ding, Q.; Okram, B.; Choi, Y.; Wojciechowski, A.; Deng, X.; Liu, G.; Fendrich, G.; Strass, A.; Vajpai, N.; Grzesiek, S.; Tuntland, T.; Liu, Y.; Bursulaya, B.; Azam, M.; Manley, P. W.; Engen, J. R.; Daley, G. Q.; Warmuth, M.; Gray, N. S. Targeting Bcr-Abl by combining allosteric with ATP-binding-site inhibitors. *Nature* **2010**, *463*, 501–506. (c) Hassan, A. Q.; Sharma, S. V.; Warmuth, M. Allosteric inhibition of

BCR-ABL. *Cell Cycle* **2010**, *9*, 3710–3714. (c) Kirkland, L. O.; McInnes, C. Non-ATP competitive kinase inhibitors as anti-tumor therapeutics. *Biochem. Pharmacol.* **2009**, *77*, 1561–1571. (d) Bogoyevitch, M. A.; Fairlie, D. P. A new paradigm for protein kinase inhibition: blocking phosphorylation without directly targeting ATP binding. *Drug Discovery Today* **2007**, *12*, 622–633.

(10) (a) Danhauser-Riedl, S.; Warmuth, M.; Druker, B. J.; Emmerich, B.; Hallek, M. Activation of Src kinases p53/56lyn and p59hck by p210bcr/abl in myeloid cells. *Cancer Res.* **1996**, *56*, 3589–3596. (b) Warmuth, M.; Damoiseaux, R.; Liu, Y.; Fabbro, D.; Gray, N. SRC family kinases: potential targets for the treatment of human cancer and leukemia. *Curr. Pharm. Des.* **2003**, *9*, 2043–2059. (c) Li, S. Src-family kinases in the development and therapy of Philadelphia chromosome-positive chronic myeloid leukemia and acute lymphoblastic leukemia. *Leuk. Lymphoma* **2008**, *49*, 19–26.

(11) (b) Schenone, S.; Manetti, F.; Botta, M. Last findings on dual inhibitors of abl and SRC tyrosine-kinases. *Mini Rev. Med. Chem.* **2007**, *7*, 191–201. (c) Martinelli, G.; Soverini, S.; Rosti, G.; Baccarani, M. Dual tyrosine kinase inhibitors in chronic myeloid leukemia. *Leukemia* **2005**, *19*, 1872–1879. (a) Schenone, S.; Bruno, O.; Botta, M.; Radi, M. New insights into small-molecule inhibitors of Bcr-Abl. *Med. Res. Rev.* **2011**, *31*, 1–41.

(12) (a) König, H.; Copland, M.; Chu, S.; Jove, R.; Holyoake, T. L.; Bhatia, R. Effects of dasatinib on SRC kinase activity and downstream intracellular signaling in primitive chronic myelogenous leukemia hematopoietic cells. *Cancer Res.* **2008**, *68*, 9624–9633.

(13) Jia, H. Y.; Wu, J. X.; Zhu, X. F.; Chen, J. M.; Yang, S. P.; Yan, H. J.; Tan, L.; Zeng, Y. X.; Huang, W. ZD6474 inhibits Src kinase leading to apoptosis of imatinib-resistant K562 cells. *Leuk. Res.* **2009**, *33*, 1512–1519.

(14) Konopleva, M.; Tabe, Y.; Zeng, Z.; Andreeff, M. Therapeutic targeting of microenvironmental interactions in leukemia: mechanisms and approaches. *Drug Resist. Updat.* **2009**, *12*, 103–113.

(15) (a) Mortensen, B. T.; Jensen, P. O.; Helledie, N.; Iversen, P. O.; Ralkkier, E.; Larsen, J. K.; Madsen, M. T. Changing bone marrow micro-environment during development of acute myeloid leukaemia in rats. *Br. J. Haematol.* **1998**, *102*, 458–464. (b) Jensen, P. O.; Mortensen, B. T.; Hodgkiss, R. J.; Iversen, P. O.; Christensen, I. J.; Helledie, N.; Larsen, J. K. Increased cellular hypoxia and reduced proliferation of both normal and leukaemic cells during progression of acute myeloid leukaemia in rats. *Cell. Prolif.* **2000**, *33*, 381–395.

(16) Giuntoli, S.; Rovida, E.; Barbetti, V.; Cipolleschi, M. G.; Olivotto, M.; Dello Sbarba, P. Hypoxia suppresses BCR/Abl and selects imatinib-insensitive progenitors within clonal CML populations. *Leukemia* **2006**, *20*, 1291–1293.

(17) Ivanovic, Z. Hypoxia or in situ normoxia: the stem cell paradigm. *J. Cell. Physiol.* **2009**, *219*, 271–275.

(18) Chow, D. C.; Wenning, L. A.; Miller, W. M.; Papoutsakis, E. T. Modeling pO(2) distributions in the bone marrow hematopoietic compartment. II. Modified Kroghian models. *Biophys. J.* **2001**, *81*, 685–696.

(19) (a) Carraro, F.; Pucci, A.; Naldini, A.; Schenone, S.; Bruno, O.; Ranise, A.; Bondavalli, F.; Brullo, C.; Fossa, P.; Menozzi, G.; Mosti, L.; Manetti, F.; Botta, M. Pyrazolo[3,4-d]pyrimidines endowed with anti-proliferative activity on ductal infiltrating carcinoma cells. *J. Med. Chem.* **2004**, *47*, 1595–1598. (b) Carraro, F.; Naldini, A.; Pucci, A.; Locatelli, G. A.; Maga, G.; Schenone, S.; Bruno, O.; Ranise, A.; Bondavalli, F.; Brullo, C.; Fossa, P.; Menozzi, G.; Mosti, L.; Modugno, M.; Tintori, C.; Manetti, F.; Botta, M. Pyrazolo[3,4-d]pyrimidines as potent antiproliferative and proapoptotic agents toward A431 and 8701-BC cells in culture via inhibition of c-Src phosphorylation. *J. Med. Chem.* **2006**, *49*, 1549–1561. (c) Manetti, F.; Santucci, A.; Locatelli, G. A.; Maga, G.; Spreafico, A.; Serchi, T.; Orlandini, M.; Bernardini, G.; Caradonna, N. P.; Spallarossa, A.; Brullo, C.; Schenone, S.; Bruno, O.; Ranise, A.; Bondavalli, F.; Hoffmann, O.; Bologna, M.; Angelucci, A.; Botta, M. Identification of a novel pyrazolo[3,4-d]pyrimidine able to inhibit cell proliferation of a human osteogenic sarcoma in vitro and in a xenograft model in mice. *J. Med. Chem.* **2007**, *50*, 5579–5588. (d) Angelucci, A.;

Schenone, S.; Gravina, G. L.; Muzi, P.; Festuccia, C.; Vicentini, C.; Botta, M.; Bologna, M. Pyrazolo[3,4-*d*]pyrimidines c-Src inhibitors reduce epidermal growth factor-induced migration in prostate cancer cells. *Eur. J. Cancer* **2006**, *42*, 2838–2845.

(20) Manetti, F.; Pucci, A.; Magnani, M.; Locatelli, G. A.; Brullo, C.; Naldini, A.; Schenone, S.; Maga, G.; Carraro, F.; Botta, M. Inhibition of Bcr-Abl phosphorylation and induction of apoptosis by pyrazolo[3,4-*d*]pyrimidines in human leukemia cells. *ChemMedChem* **2007**, *2*, 343–353.

(21) (a) Santucci, M. A.; Corradi, V.; Mancini, M.; Manetti, F.; Radi, M.; Schenone, S.; Botta, M. C6-unsubstituted pyrazolo[3,4-*d*]pyrimidines are dual Src/Abl inhibitors effective against imatinib mesylate resistant chronic myeloid leukemia cell lines. *ChemMedChem* **2009**, *4*, 118–126. (b) Santucci, M. A.; Mancini, M.; Corradi, V.; Iacobucci, I.; Martinelli, G.; Botta, M.; Schenone, S. New SRC/ABL inhibitors for chronic myeloid leukemia therapy show selectivity for T3151 ABL mutant CD34(+) cells. *Invest. New Drugs* **2010**, *28*, 876–878. (c) Schenone, S.; Brullo, C.; Botta, M. New opportunities to treat the T3151-Bcr-Abl mutant in chronic myeloid leukaemia: tyrosine kinase inhibitors and molecules that act by alternative mechanisms. *Curr. Med. Chem.* **2010**, *17*, 1220–1245.

(22) (a) Tintori, C.; Magnani, M.; Schenone, S.; Botta, M. Docking, 3D-QSAR studies and in silico ADME prediction on c-Src tyrosine kinase inhibitors. *Eur. J. Med. Chem.* **2009**, *44*, 990–1000. (b) Schenone, S.; Brullo, C.; Bruno, O.; Bondavalli, F.; Mosti, L.; Maga, G.; Crespan, E.; Carraro, F.; Manetti, F.; Tintori, C.; Botta, M. Synthesis, biological evaluation and docking studies of 4-amino substituted 1*H*-pyrazolo[3,4-*d*]pyrimidines. *Eur. J. Med. Chem.* **2008**, *43*, 2665–2676. (c) Manetti, F.; Brullo, C.; Magnani, M.; Mosci, F.; Chelli, B.; Crespan, E.; Schenone, S.; Naldini, A.; Bruno, O.; Trincavelli, M. L.; Maga, G.; Carraro, F.; Martini, C.; Bondavalli, F.; Botta, M. Structure-based optimization of pyrazolo[3,4-*d*]pyrimidines as Abl inhibitors and antiproliferative agents toward human leukemia cell lines. *J. Med. Chem.* **2008**, *51*, 1252–1259.

(23) *Discovery Studio*, version 2.5; Accelrys Inc.: San Diego, CA, 2007.

(24) Wu, T. Y.; Schultz, P. G.; Ding, S. One-pot two-step microwave-assisted reaction in constructing 4,5-disubstituted pyrazolopyrimidines. *Org. Lett.* **2003**, *20*, 3587–3590.

(25) Asosingh, K.; De Raevae, H.; de Ridder, M.; Storme, G. A.; Willems, A.; Van Riet, I.; Van Camp, B.; Vanderkerken, K. Role of the hypoxic bone marrow microenvironment in ST2MM murine myeloma tumor progression. *Haematologica* **2005**, *90*, 810–817.

(26) Takeuchi, M.; Kimura, S.; Kuroda, J.; Ashihara, E.; Kawatani, M.; Osada, H.; Umezawa, K.; Yasui, E.; Imoto, M.; Tsuruo, T.; Yokota, A.; Tanaka, R.; Nagao, R.; Nakahata, T.; Fujiyama, Y.; Maekawa, T. Glyoxalase-I is a novel target against Bcr-Abl+ leukemic cells acquiring stem-like characteristics in a hypoxic environment. *Cell. Death Differ.* **2010**, *17*, 1211–1220.

(27) Ke, Q.; Costa, M. Hypoxia-inducible factor-1 (HIF-1). *Mol. Pharmacol.* **2006**, *70*, 1469–1480.

(28) Data not shown.

(29) Warmuth, M.; Damoiseaux, R.; Liu, Y.; Fabbro, D.; Gray, N. SRC family kinases: potential targets for the treatment of human cancer and leukemia. *Curr. Pharm. Des.* **2003**, *9*, 2043–2059.

(30) (a) Tureci, O.; Sahin, U.; Vollmar, E.; Siemer, S.; Gottert, E.; Seitz, G.; Parkkila, A. K.; Shah, G. N.; Grubb, J. H.; Pfreundschuh, M.; Sly, W. S. Human carbonic anhydrase XII: cDNA cloning, expression, and chromosomal localization of a carbonic anhydrase gene that is overexpressed in some renal cell cancers. *Proc. Natl. Acad. Sci. U.S.A.* **1998**, *95*, 7608–7613. (b) Zavada, J.; Zavadova, Z.; Pastorekova, S.; Ciampor, F.; Pastorek, J.; Zelnik, V. Expression of MaTu-MN protein in human tumor cultures and in clinical specimens. *Int. J. Cancer* **1993**, *54*, 268–274. (c) Pastorek, J.; Pastorekova, S.; Callebaut, I.; Mornon, J. P.; Zelnik, V.; Opavsky, R.; Zat'ovicová, M.; Liao, S.; Portetelle, D.; Stanbridge, E. J.; Zavada, J.; Burny, A.; Kettmann, R. Cloning and characterization of MN, a human tumor-associated protein with a domain homologous to carbonic anhydrase and a putative helix-loop-helix DNA binding segment. *Oncogene* **1994**, *9*, 2877–2888.

(31) (a) Poulsen, S. A. Carbonic anhydrase inhibition as a cancer therapy: a review of patent literature, 2007–2009. *Expert Opin. Ther. Pat.* **2010**, *20*, 795–806. (b) Chen, C. L.; Chu, J. S.; Su, W. C.; Huang, S. C.; Lee, W. Y. Hypoxia and metabolic phenotypes during breast carcinogenesis: expression of HIF-1 α , GLUT1, and CAIX. *Virchows Arch.* **2010**, *457*, 53–61. (c) Ilie, M.; Mazure, N. M.; Hofman, V.; Ammadi, R. E.; Ortholan, C.; Bonnetaud, C.; Havet, K.; Venissac, N.; Mograbi, B.; Mouroux, J.; Pouyssegur, J.; Hofman, P. High levels of carbonic anhydrase IX in tumour tissue and plasma are biomarkers of poor prognostic in patients with non-small cell lung cancer. *Br. J. Cancer.* **2010**, *102*, 1627–1635.

(32) (a) Kansy, M. F.; Senner, K.; Gubernator, K. Physicochemical high throughput screening, parallel artificial membrane permeation assay in the description of passive absorption processes. *J. Med. Chem.* **1998**, *41*, 1007–1010. (b) Avdeef, A. The rise of PAMPA. *Expert Opin. Drug Met.* **2005**, *1*, 325–342.

(33) Di, L.; Kerns, E. H. Application of pharmaceutical profiling assays for optimization of drug-like properties. *Curr. Opin. Drug Discovery Dev.* **2005**, *8*, 495–504.

(34) Details on the synthesis of compound **19** are reported in Supporting Informations.

(35) Dreassi, E.; Zizzari, A. T.; Falchi, F.; Schenone, S.; Santucci, A.; Maga, G.; Botta, M. Determination of permeability and lipophilicity of pyrazolo-pyrimidine tyrosine kinase inhibitors and correlation with biological data. *Eur. J. Med. Chem.* **2009**, *44*, 3712–3717.

(36) (a) Avdeef, A. High-throughput measurements of solubility profiles. Pharmacokinetic optimization in drug research: biological, physicochemical, and computational strategies. LogP2000, Lipophilicity Symposium, 2nd, Lausanne, Switzerland, March 5–9, 2000; pp 305–325. (b) Bard, B.; Martel, S.; Carrupt, P. A. High throughput UV method for the estimation of thermodynamic solubility and the determination of the solubility in biorelevant media. *Eur. J. Pharm. Sci.* **2008**, *33*, 230–240. (c) Connors, K. A.; Mollica, J. A., Jr. Theoretical analysis of comparative studies of complex formation. *J. Pharm. Sci.* **1966**, *55*, 772–780.

(37) Cruciani, G.; Carosati, E.; De Boeck, B.; Ethirajulu, K.; Mackie, C.; Howe, T.; Vianello, R. MetaSite: Understanding metabolism in human cytochromes from the perspective of the chemist. *J. Med. Chem.* **2005**, *48*, 6970–6979.

(38) (a) Jones, G.; Willett, P.; Glen, R. C. Molecular recognition of receptor sites using a genetic algorithm with a description of desolvation. *J. Mol. Biol.* **1995**, *245*, 43–53. (b) Jones, G.; Willett, P.; Glen, R. C.; Leach, A. R.; Taylor, R. Development and validation of a genetic algorithm for flexible docking. *J. Mol. Biol.* **1997**, *267*, 727–748. (c) Verdonk, M. L.; Cole, J. C.; Hartshorn, M. J.; Murray, C. W.; Taylor, R. D. Improved protein-ligand docking using GOLD. *Proteins* **2003**, *52*, 609–623.

(39) *MacroModel*, version 8.5; Schrodinger, LLC: New York, 2003.

(40) Nagar, B.; Bornmann, W. G.; Pellicena, P.; Schindler, T.; Veach, D. R.; Miller, W. T.; Clarkson, B.; Kuriyan, J. Crystal structures of the kinase domain of c-Abl in complex with the small molecule inhibitors PD173955 and imatinib (STI-571). *Cancer Res.* **2002**, *62*, 4236–4243.

(41) Breitenlechner, C. B.; Kairies, N. A.; Honold, K.; Scheiblich, S.; Koll, H.; Greiter, E.; Koch, S.; Schafer, W.; Huber, R.; Engh, R. A. Crystal structures of active SRC kinase domain complexes. *J. Mol. Biol.* **2005**, *353*, 222–231.

(42) Cowan-Jacob, S. W.; Fendrich, G.; Manley, P. W.; Jahnke, W.; Fabbro, D.; Liebetanz, J.; Meyer, T. The crystal structure of a c-Src complex in an active conformation suggests possible steps in c-Src activation. *Structure* **2005**, *13*, 861–871.

(43) Wohnsland, F.; Faller, B. High-throughput permeability pH profile and high-throughput alkane/water log P with artificial membranes. *J. Med. Chem.* **2001**, *44*, 923–930.

(44) Sugano, K.; Hamada, H.; Machida, M.; Ushio, H. High throughput prediction of oral absorption: improvement of the composition of the lipid solution used in parallel artificial membrane permeation assay. *J. Biomol. Screen.* **2001**, *6*, 189–196.

(45) D'Elia, P.; De Matteis, F.; Dragoni, S.; Shah, A.; Sgaragli, G.; Valoti, M. DP7, a novel dihydropyridine multidrug resistance reverter,

shows only weak inhibitory activity on human CYP3A enzyme(s). *Eur. J. Pharmacol.* **2009**, *614*, 7–13.

(46) (a) Hudig, D.; Djobadze, M.; Redelman, D.; Mendelsohn, J. Active tumor cell resistance to human natural killer lymphocyte attack. *Cancer Res.* **1981**, *41*, 2803–2808. (b) Ogura, M.; Morishima, Y.; Ohno, R.; Kato, Y.; Hirabayashi, N.; Nagura, H.; Saito, H. Establishment of a novel human megakaryoblastic leukemia cell line, MEG-01, with positive Philadelphia chromosome. *Blood* **1985**, *66*, 1384–1392. (c) Kishi, K. A new leukemia cell line with Philadelphia chromosome characterized as basophil precursors. *Leuk. Res.* **1985**, *9*, 381–390.

(47) Naldini, A.; Carraro, F. Hypoxia modulates cyclin and cytokine expression and inhibits peripheral mononuclear cell proliferation. *J. Cell. Physiol.* **1999**, *181*, 448–454.

(48) Carraro, F.; Pucci, A.; Pellegrini, M.; Pelicci, P. G.; Baldari, C. T.; Naldini, A. P66Shc is involved in promoting HIF-1 α accumulation and cell death in hypoxic T cells. *J. Cell. Physiol.* **2007**, *211*, 439–447.

(49) Vandesompele, J.; De Preter, K.; Pattyn, F.; Poppe, B.; Van Roy, N.; De Paepe, A.; Speleman, F. Accurate normalization of real-time quantitative RT-PCR data by geometric averaging of multiple internal control genes. *Genome Biol.* **2002**, *3*, 1–12.